

Rowan University

Rowan Digital Works


Theses and Dissertations

5-24-2018

Perovskite solar cells fabricated via scalable dip coating methods

Joseph F. Iannello
Rowan University

Follow this and additional works at: <https://rdw.rowan.edu/etd>

 Part of the [Materials Science and Engineering Commons](#), [Mechanical Engineering Commons](#), and the [Power and Energy Commons](#)

Recommended Citation

Iannello, Joseph F., "Perovskite solar cells fabricated via scalable dip coating methods" (2018). *Theses and Dissertations*. 2569.

<https://rdw.rowan.edu/etd/2569>

This Thesis is brought to you for free and open access by Rowan Digital Works. It has been accepted for inclusion in Theses and Dissertations by an authorized administrator of Rowan Digital Works. For more information, please contact graduateresearch@rowan.edu.

**PEROVSKITE SOLAR CELLS FABRICATED VIA SCALABLE DIP COATING
METHODS**

by

Joseph F. Iannello

A Thesis

Submitted to the
Department of Mechanical Engineering
Henry M. Rowan College of Engineering
In partial fulfillment of the requirement
For the degree of
Master of Science in Mechanical Engineering
At
Rowan University
April 19, 2018

Thesis Advisor: Dr. Wei Xue, Ph.D.

Acknowledgements

I would like to express my appreciation to my advisor, Dr. Wei Xue, for allowing me the opportunity to work in his research group. This work would not have been completed without his insightful guidance and patience for which I am deeply indebted.

I would like to thank Dr. Kandalam Ramanujachary for his continued investment in this research project. Without which, none of this would be possible.

I would like to thank my thesis committee members, Dr. Jeffrey Hettinger and Francis M.Haas for their help and their time that was contributed to this project.

In addition, I would like to thank Pat Jackson, Chris Kelbon, John Fogelin, and Carl Lunk for their time and dedication spent training me on proper laboratory practices.

Lastly, I would like to thank all of my friends and family, for their continued support throughout the years.

Abstract

Joseph Iannello
PEROVSKITE SOLAR CELLS FABRICATED VIA SCALABLE DIP COATING
METHODS
2017-2018
Wei Xue, Ph.D.
Master of Science in Mechanical Engineering

Perovskite solar cells present the possibility for less expensive electricity generation, through the use of low cost materials and fabrication methods relative to current silicon-based technology. Many current methods of fabricating thin film perovskite solar cells focus on spin-coating, which inherently lacks scalability due to particle conglomeration, poor uniformity over a larger area, and safety concerns. Dip-coating, an alternative to spin-coating, which is explored here addresses these issues which limit scalability. Each individual layer can be separately synthesized, deposited, and characterized, which leads towards scalability. Choosing only the best results from each independent layer allowed progress to the creation of a sandwich style perovskite cell fabricated through dip coating. By using a quartz crystal microbalance, the thicknesses of these uniform films has been determined to be in the desired range of under one micron. Currently, there is a photo response present, with a maximum produced voltage of 500 mV. The methods presented here create an initial starting point for the large scale manufacturing of dip coated perovskite solar cells.

Table of Contents

Abstract	iv
List of Figures	vii
Chapter 1: Introduction	1
1.1 Motivation	1
1.2 Background	6
1.3 Objectives	11
Chapter 2: Electron Transport Layer	14
2.1 Zinc Oxide Nano-Rod Fabrication	14
2.2 Sol-Gel Method	16
2.3 Zinc Oxide Nanoparticles.....	19
2.4. Film Thickness and Purity.....	21
Chapter 3: Lead Iodide and Perovskite.....	24
3.1 Lead Iodide.....	24
3.2 Fabrication of Lead Iodide Films Without a Solvent.....	24
3.3 Fabrication of Lead Iodide Films With a Solvent.....	27
3.3.1. Spray coating.....	27
3.3.2. Dip coating.....	30
3.4 Perovskite Synthesis.....	33
Chapter 4: Hole Transport Layer, Top Electrode and Testing.....	37

Table of Contents (Continued)

4.1 Spiro-MeOTAD	37
4.2 Copper(I) Thiocyanate	39
4.3 Top Electrode	41
4.4 Testing	42
Chapter 5: Conclusions and Future Works	43
References	48

List of Figures

Figure	Page
Figure 1. Energy consumed globally, by type, for the year of 2017, in terawatt hours according to the BP statistical review of world energy[1].....	2
Figure 2. The predicted LCOE for various types of energy generation according to the eia[2].	3
Figure 3. Best research cell efficiencies from 1975 until 2017 from the National Renewable Energy Laboratory [3].....	4
Figure 4. The method of fabricating pure silicon wafers is known as the Czochralski process.....	5
Figure 5. The general structure of a perovskite crystal.....	7
Figure 6. The general device structure of a perovskite solar cell.	8
Figure 7. This energy level diagram summarizes the energy level of materials used in perovskite solar cells relative to vacuum.	9
Figure 8. Current spin coating methods rely on a two-step method which involves spinning substrates at high rpm's.....	11
Figure 9. Fabrication of a perovskite solar cell through dip coating.	13
Figure 10. Zinc oxide nano-rods on a glass substrate. Individual rods can be seen from top-down, though the film lacks uniformity.	15
Figure 11. Zinc oxide films on a glass substrate. Image (a) is an overall view while image (b) is a higher magnification.	17
Figure 12. Zinc oxide films. Image (a) is after one dip, image (b) is after four dips.....	18
Figure 13. Zinc oxide films from stock nano-particles, (a) presents and overall view while (b) is more magnified.....	20

Figure 14. A film fabricated using synthesized zinc oxide nanoparticles. Image (a) presents an overall view, while image (b) shows a closer look.	21
Figure 15. The average thickness of a zinc oxide film after successive dips.	22
Figure 16. FTIR of the synthesized zinc oxide powder. The lack of any spectra lines at 1500 and 750 indicates a high purity of zinc oxide.	23
Figure 17. Lead Iodide films fabricated using two step dip coating with no solvent.	26
Figure 18. SEM images of colloidal lead iodide films dip coated without a solvent.	27
Figure 19. Spray coated lead iodide film fabricated by spraying three times.	29
Figure 20. Spray coated lead iodide film fabricated by spraying nine times.	30
Figure 21. Dip Coated lead iodide film using a concentration of 460 mg ml ⁻¹ lead iodide in DMF.	31
Figure 22. Average thickness of a lead iodide film at 230 mg ml ⁻¹ after one and two dips.	32
Figure 23. Dip coated lead iodide film fabricated using a concentration of 230 mg ml ⁻¹ lead iodide in DMF.	33
Figure 24. An SEM image and its corresponding X-ray diffraction pattern represented by the two-step dip coated MAI perovskite film.	34
Figure 25. A comparison of perovskite films annealed at two separate temperatures.	36
Figure 26. A Spiro-MeOTAD film on top of perovskite.	39
Figure 27. A CuSCN film on top of perovskite.	41

Chapter 1

Introduction

1.1 Motivation

The BP statistical review reports that during the calendar year 2016, 18.2 TW of energy was consumed globally[1]. 3.06% of this energy consumed was generated by renewable sources, other than hydroelectricity, or nuclear power. Solar energy was responsible for only 0.048% of total energy consumed, which amounts to 8.79 GW. Figure 1 presents a detailed breakdown of energy consumption by each produced method. Each year, 23000 TW of available energy hits the Earth's surface as radiation from the sun, which far exceeds the consumption of the Human population. The largest obstacle for solar energy production to overcome is cost.

The Levelised Cost of Electricity (LCOE) is how different methods of electricity generation are compared to one another in a consistent way. In order for solar energy production to become viable on a larger scale, the LCOE must drop below or near that of other current methods of production. Using current numbers and market trends, the Energy Information Administration (eia) has published a number of accurate predictions of the LOCE of different methods of electricity generation [2]. Figure 2 shows the estimated LOCE for 2022 as a simple average of regional values, based on projected capacity for new generation resources, for plants entering service. We can see that conventional combined cycle natural gas is predicted to cost \$57.30 per MWh as opposed

to PV solar, which is \$85.00 per MW. Even with four years of technological advancements, this puts solar at a cost of 148% of conventional combined cycle natural gas, which is one of the biggest reasons for finding ways to reduce costs of photovoltaic cells even further.

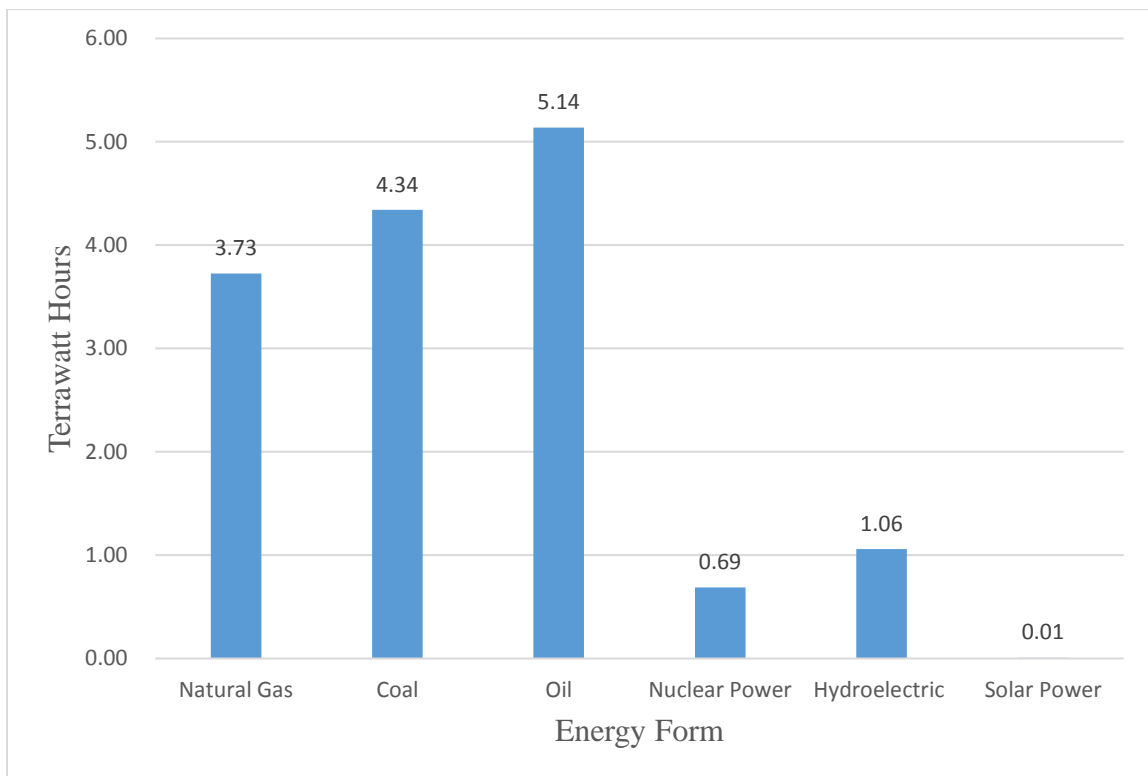


Figure 1. Energy consumed globally, by type, for the year of 2017, in terawatt hours according to the BP statistical review of world energy[1].

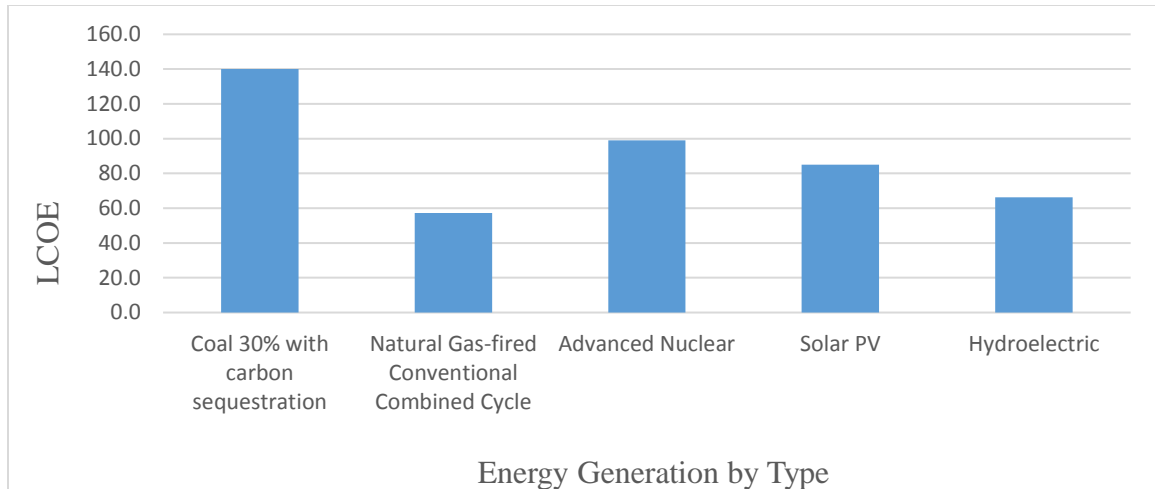


Figure 2. The predicted LCOE for various types of energy generation according to the eia[2].

Currently produced solar panels are part of what is called the first generation of solar panels. These are made of silicon, and come in two types, monocrystalline, and polycrystalline. The biggest differences between these two types are efficiency, and production cost. Figure 3 shows the current best research efficiencies photovoltaic cells. This is a yearly graph which details current best production methods, from 1975 until 2017. Looking at the year for 2017, the blue line represents silicon cells, and the highest efficiency is for monocrystalline, at around 28%, while polycrystalline are slightly lower, at about 23% [3]. Figure 4 shows the creation of monocrystalline panels using the Czochralski process, which is one of the main reasons why prices have not fallen below the LCOE needed. Creating a monocrystalline silicon wafer is the first step in fabricating conventional solar panels. Quartz sand is heated and purified, then a seed crystal is inserted into the molten bath. This seed crystal is slowly drawn out and spun, creating a monocrystalline ingot of nearly pure silicon. The ingot is then cut into micron-sized

wafers, etched, and polished, before being sent to another facility where dopants are added and the final panel is constructed.

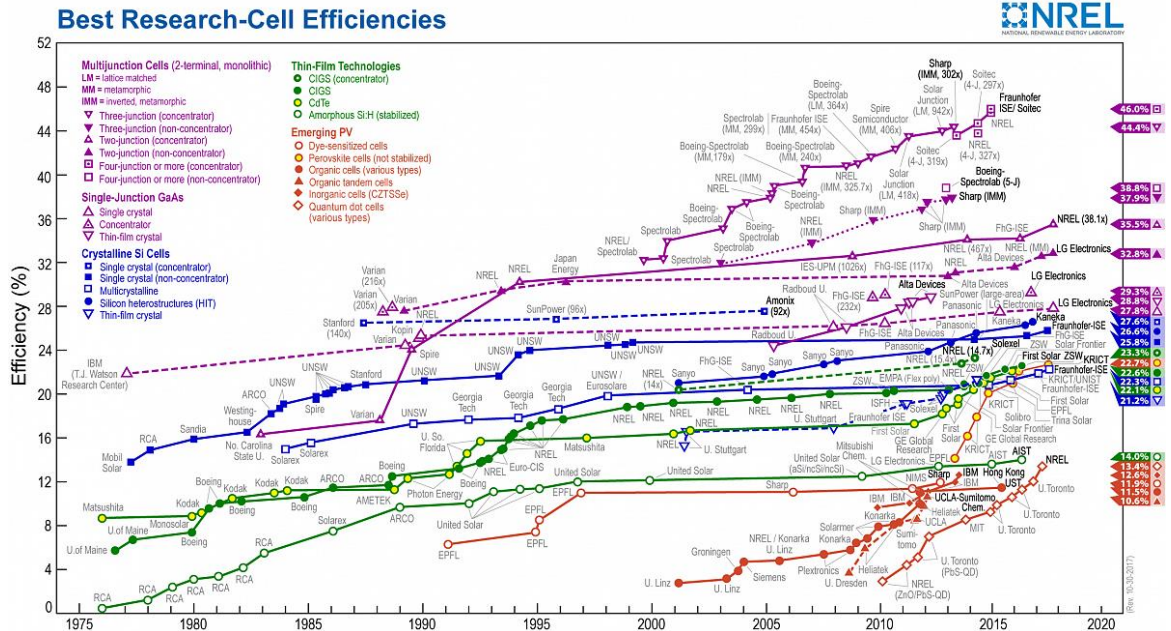


Figure 3. Best research cell efficiencies from 1975 until 2017 from the National Renewable Energy Laboratory [3].

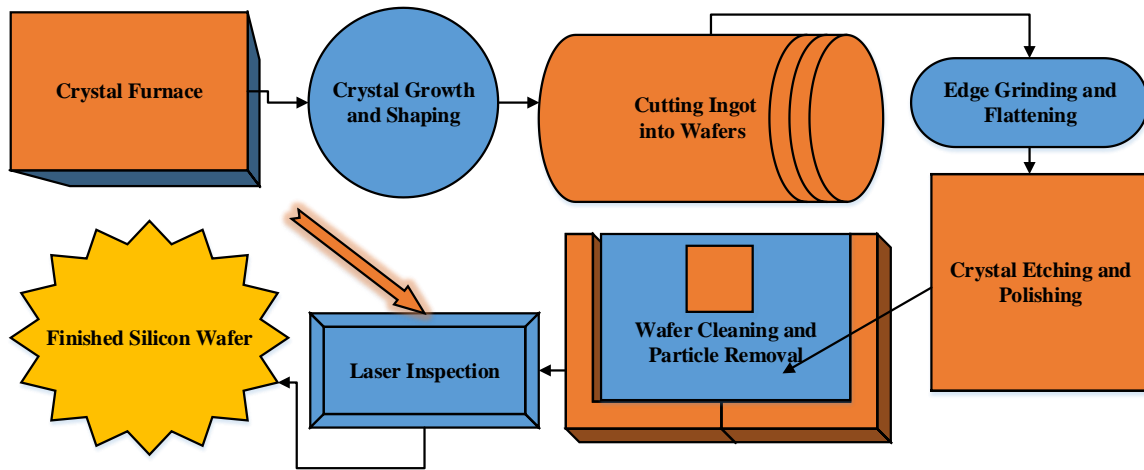


Figure 4. The method of fabricating pure silicon wafers is known as the Czochralski process.

The second generation of solar cells are thin film solar cells, usually fabricated using the element cadmium. While efficiencies are comparable to those of silicon, the rarity and high toxicity of cadmium has prevented this technology from reaching its full potential, and second generation panels only make up about 10% of the current market share. The third generation of photovoltaic cells include dye sensitized solar cells (DSSCs), quantum dots, and perovskite solar cells. While DSSCs and quantum dots have showed promise, they have their limitations which must be overcome before they can be brought to market. Most notably, DSSCs contain liquid and biological matter, which leave them open to decomposing and vulnerable to the elements. Quantum dots, while individually tunable, are expensive to make, and highly toxic. Perovskite, the third material classified as a Generation-3 solar cell material, has shown an exceptional increase in performance since its inception. Figure 3 shows this marked increase in

efficiency. The orange line with yellow circles represents perovskites, in 8 years, the efficiency of perovskite solar cells has risen almost 20%. The first perovskite cell was described in 2009, and had an efficiency of 3.8% [4]. Since then, advancements in this field have improved drastically, with the highest verified efficiency now at 22.7%, measured in 2017 [3]. This large increase in efficiency in such a short time, combined with low material cost, are two of the biggest reasons why perovskite solar cells have attracted so much attention.

1.2 Background

Perovskite was first discovered in 1839 by Gustav Rose in the Ural Mountains of Russia, and was named after a famous geologist at the time, Lev Perovski. The discovered mineral had a chemical formula of CaTiO_3 . Figure 5 shows this general chemical formula of ABX_3 , which leads to the ideal perovskite structure, within a certain tolerance [5]. This tolerance is known as the Goldschmidt tolerance factor, which was first described by Victor Moritz Goldschmidt in 1926. The Goldschmidt tolerance factor is based on the ionic radii of the elements that make up the perovskite crystal, and is defined by the following equation [6, 7],

$$t = \frac{r_A + r_0}{\sqrt{2}(r_B + r_0)} \quad (1.1)$$

where r_A is the radius of the A-cation, r_B is the radius of the B-cation, and r_0 is the radius of the anion. An ideal cubic perovskite structure of the unit cell (a) is defined by the following equation [5].

$$a = \sqrt{2}(r_A + r_0) = 2(r_B + r_0) \quad (1.2)$$

A stable, cubic, perovskite structure occurs if $0.89 < t < 1$, which means that the cations are of ideal size [5].

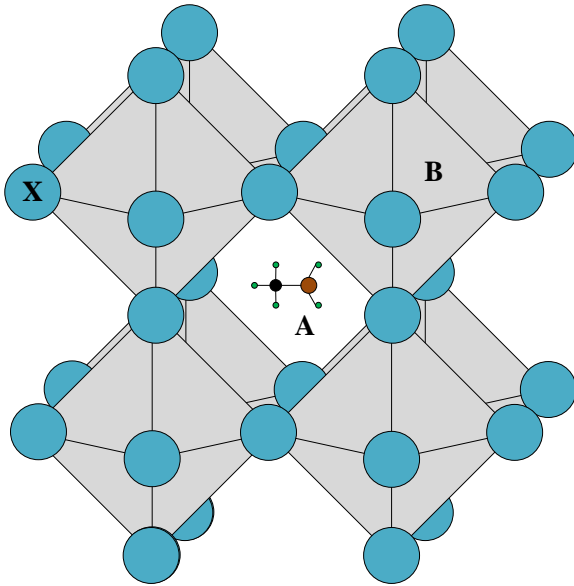


Figure 5. The general structure of a perovskite crystal.

Perovskite solar cells are constructed in a sandwich style, using multiple layers of thin films to harvest light [8]. Figure 6 shows the general style of a perovskite cell, which has remained relatively unchanged since their inception. These cells work on the principal of the photoelectric effect and exciton generation. Excitons are generated in the perovskite by light, once generated, the holes and electrons follow the path of least resistance through their respective layers. Electrons are then collected on the cathode, and

holes on the anode, creating a potential difference. When a load is applied, this potential difference can be used to power it.

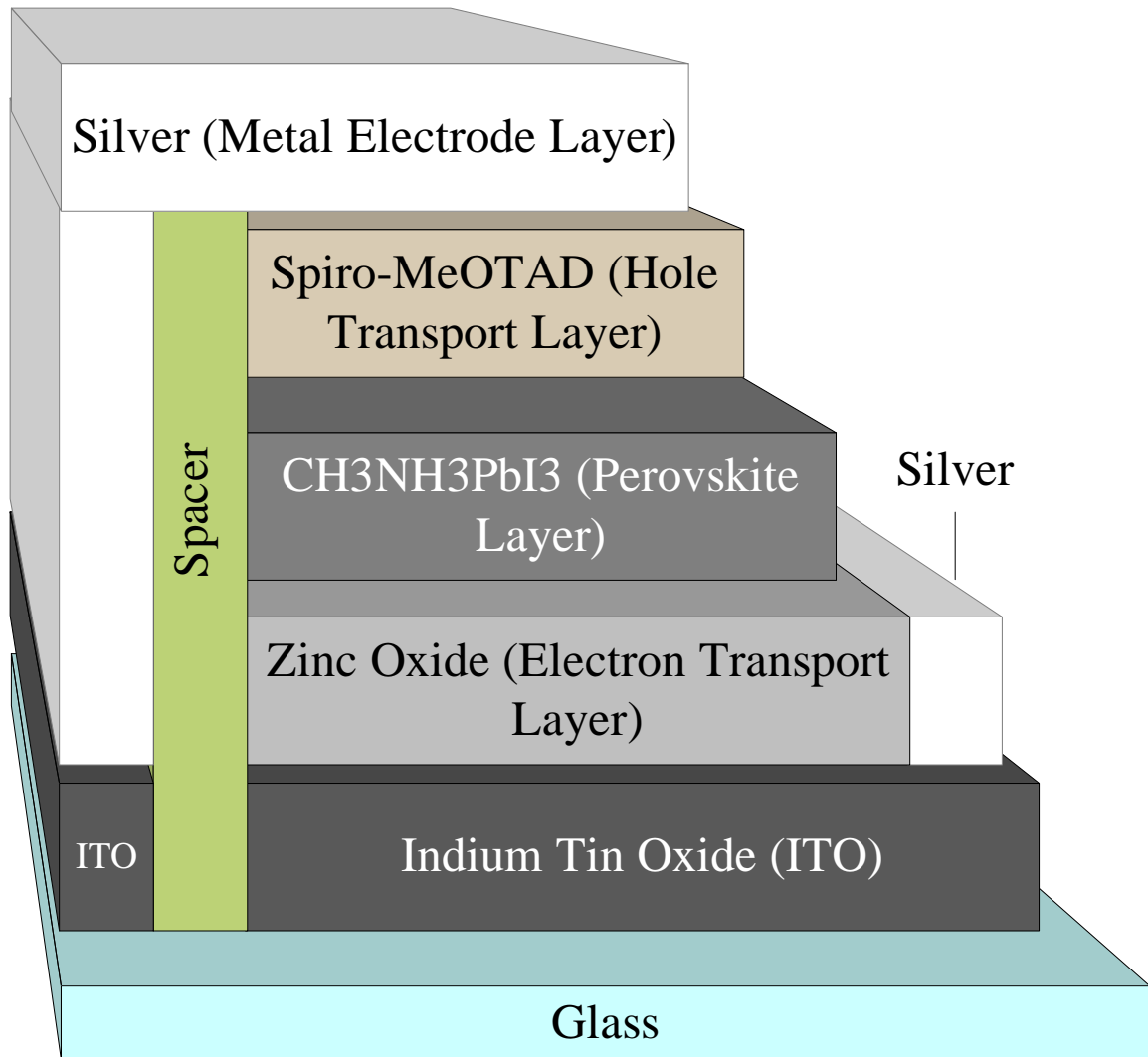


Figure 6. The general device structure of a perovskite solar cell.

Figure 7 shows an energy level diagram of a perovskite solar cell, indicating how the photoelectric effect can be utilized to generate electricity [9]. By utilizing the energy level of different materials, a perovskite solar cell can cause electrons and holes to be extracted on opposite sides of the cell, creating a potential difference. Electrons and holes will follow the path of least resistance through the cell, so the differences in energy level should be minimized to ensure maximum device performance.

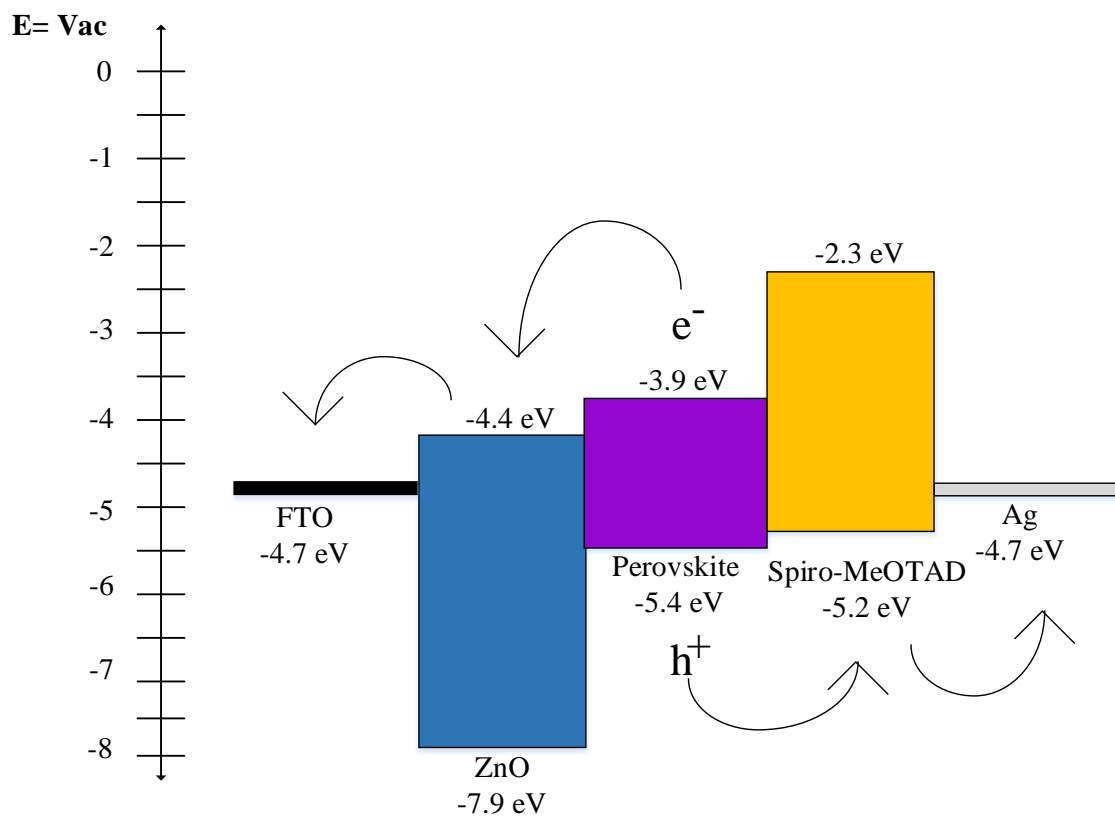
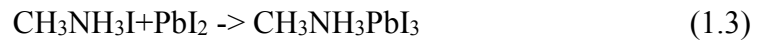


Figure 7. This energy level diagram summarizes the energy level of materials used in perovskite solar cells relative to vacuum.

The Shockley-Queisser limit for a single junction solar cell defines a maximum efficiency of 33.7%, with a band-gap of 1.37 eV [10]. The first, most commonly used, and most efficient perovskites so far, have a chemical formula of $\text{CH}_3\text{NH}_3\text{PbI}_3$, which is in line with the general ABX_3 formula for a perovskite [4, 8, 11]. These perovskites are formed according to the following reaction



$\text{CH}_3\text{NH}_3\text{I}$ is also known as methylammonium iodide or MAI. To date, many successful MAI lead-based perovskite cells have a band-gap of 1.56 eV, corresponding to a theoretical maximum efficiency of 31.3 [12]. This is comparable to silicon, which has a band-gap of 1.1 eV and a maximum theoretical efficiency of about 32%. Band-gaps of perovskites can be tuned anywhere from 1.17 – 1.56 by changing doping ratios of Sn^{+2} and Pb^{+2} [13]. This tunability also allows for a variety of differences between designs based on the electron transport layer, and the hole transport layer, as well as allowing for the possibility multi-junction perovskite solar cells.

Current, most high performance perovskite solar cells are fabricated using a method known as spin coating [8, 14]. Figure 8 shows a current method of spin coating, which revolves around the concept of spinning substrates at a high speed to produce uniform thin films. While spin coating produces reliable results which are replicated easily in a laboratory setting, spin coating fundamentally lacks scalability due to a variety of factors. One large issue is that spin coating only produces uniform films on small areas. As the desired area becomes larger, particles start to aggregate and produce large clumps in lines radially along the substrate. Another issue is safety, the larger the substrate, the greater the risk of damage if something fails and the substrate becomes

unattached to the spin coater.

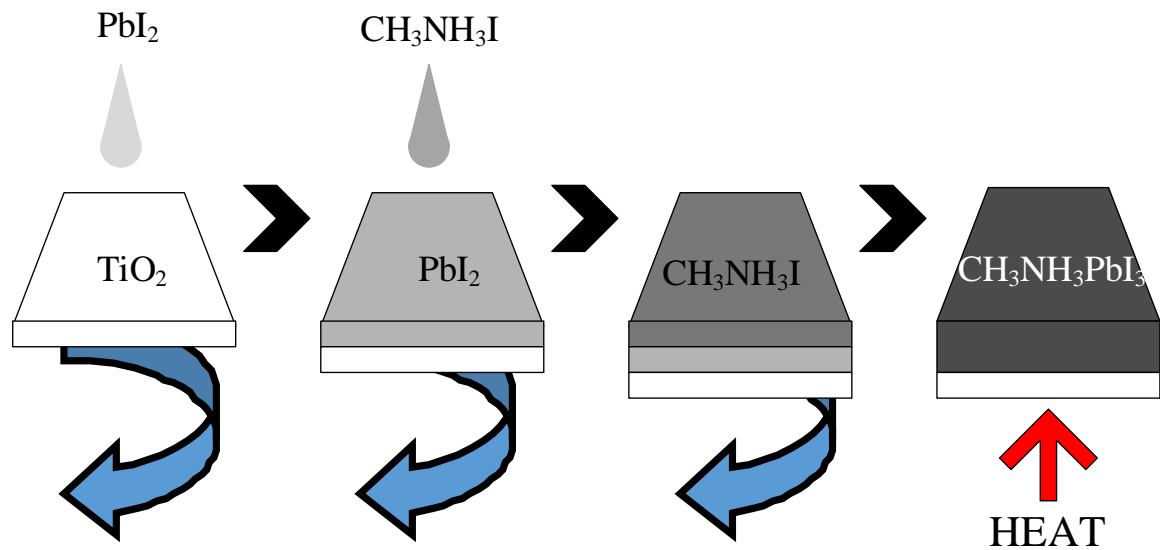


Figure 8. Current spin coating methods rely on a two-step method which involves spinning substrates at high rpm's.

1.3 Objectives

As spin-coating inherently lacks scalability, other alternatives must be investigated. Current published alternatives include roll-to-roll processing, spray coating, and slot-die coating [15-18]. Slot-die coating is a typical large-scale manufacturing process. The desired chemical, in this case, lead iodide, is sent through a small channel, which is the slot, with an additional slot blowing out an inert gas, usually nitrogen, which follows immediately behind it. By taking these slots and quickly moving them across a substrate, thin films of lead iodide of relatively good uniformity can be produced. Though

advancements have been made using these processing methods, producing uniform films which cover a large area have still been a challenge. Stability is also an issue, as ambient moisture will degrade the perovskite, all devices must be encapsulated to ensure there is no degradation. The primary objectives of investigating the large scale manufacturing of perovskites is the purpose of this thesis, and is done so through dip-coating. By fabricating, characterizing, and optimizing each individual layer of a perovskite solar cell, an entire cell can be fabricated through dip-coating. Figure 9 shows the general process of dip coating for an entire perovskite cells, except the top electrode. A substrate is dunked into a container of the desired chemical, and then dried. Depending on the number of dips, concentration of the solution, dipping angle, and drying angle, thin films of varying thicknesses and uniformities can be fabricated. By choosing the most uniform films for each step and continuing, a clear photo response is observed.

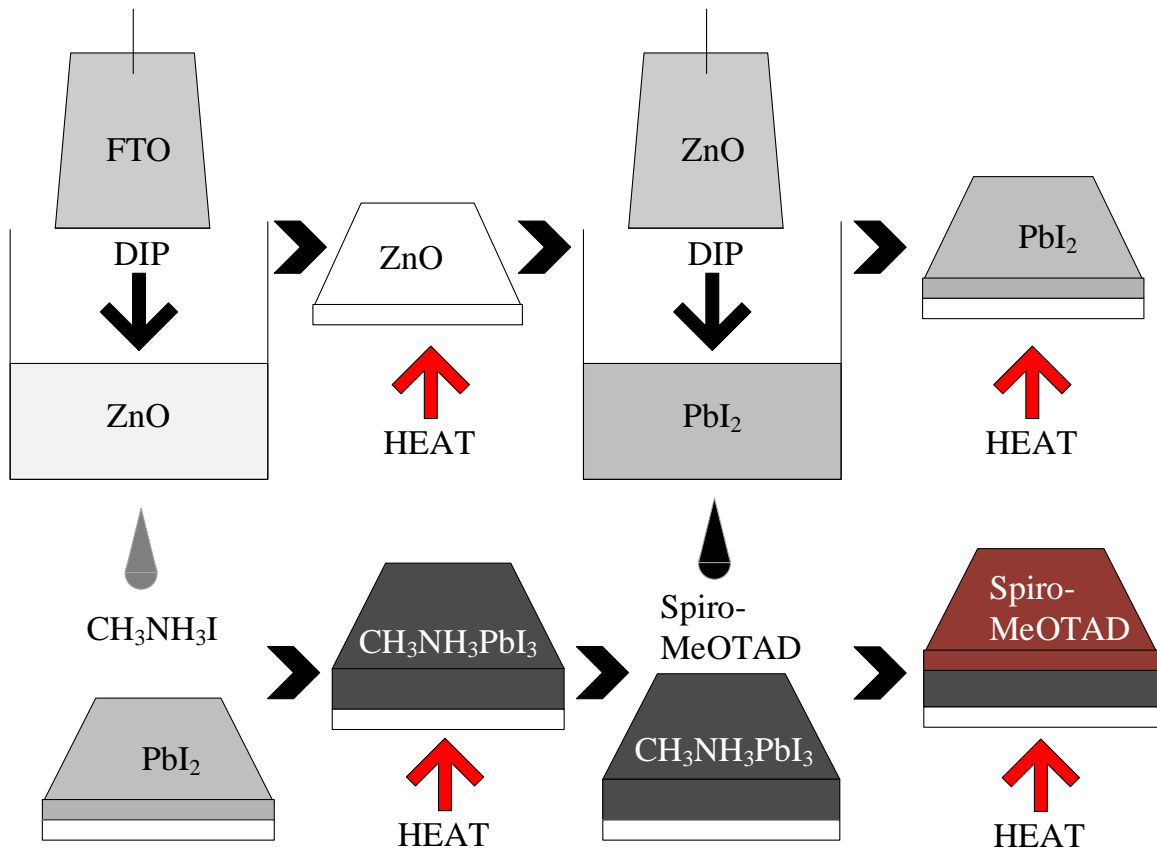


Figure 9. Fabrication of a perovskite solar cell through dip coating.

Chapter 2

Electron Transport Layer

Described in the following chapter are multiple synthesis methods for different types of zinc oxide particles, which can be used a material for the electron transport layer. Titanium dioxide was also investigated, but due to the high temperature required for annealing, zinc oxide was chosen as the desired material. Types of zinc oxide particles include nano-rods, stock nanoparticles, and synthesized nanoparticles. As uniformity is the biggest issue for large-scale manufacturing, a scanning electron microscope was used to identify topographical information about the deposited layers. The most uniform layer, within the desired thickness, was fabricated using synthesized zinc oxide nano-particles.

2.1 Zinc Oxide Nano-Rod Fabrication

Referring back to Figure 6, there are various layers involved in a perovskite solar cell. Each of these layers are composed of different materials, some of which must first be synthesized prior to deposition. A reasonable starting position was the electron transport layer (ETL), which is most often composed of either titanium dioxide or zinc oxide [19-22]. As low cost and low temperature were objectives, it was decided that zinc oxide would be the material of choice. This is due to the fact that titanium dioxide thin films require a very high annealing temperature, on the order of 400-500°C [23-25]. A high temperature annealing step would not only drive up costs, but also limit the substrates on which the films can be deposited. As a bendable cell on a plastic substrate was a desired outcome, zinc oxide was chosen.

Known for their high carrier concentration, zinc oxide nano-rod thin films were the starting point for this layer [26, 27]. Following known methods, zinc oxide nano-rod

thin films were produced on non-coated, and ITO-coated glass substrates [28-30]. Though these methods produced relatively uniform films, the process took a relatively long time, on the order of days. As a long fabrication period adds to costs, a different method of fabrication was investigated [31, 32]. Though zinc oxide nano-rods were produced in a much quicker fashion, this method required gold nanoparticles to be sputter coated beforehand, as this additional step added a much higher cost to fabrication. Figure 10 shows a film produced using this method and its lack of uniformity. Due to these two issues, nanoparticles were investigated instead of nano-rods.

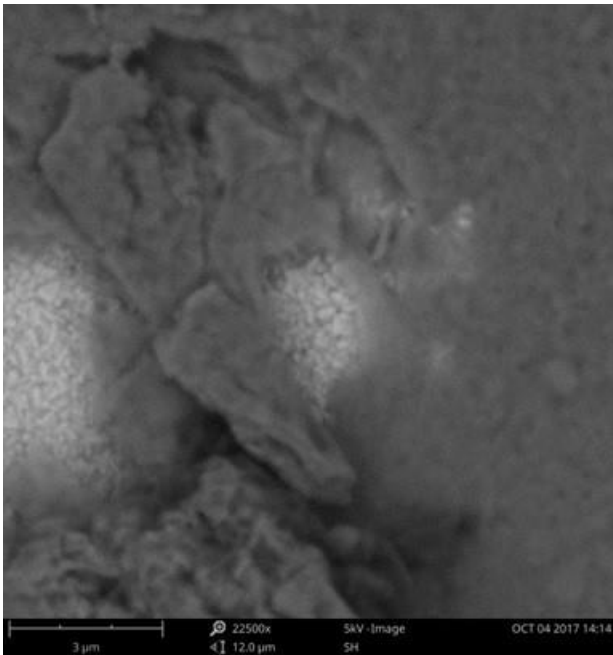


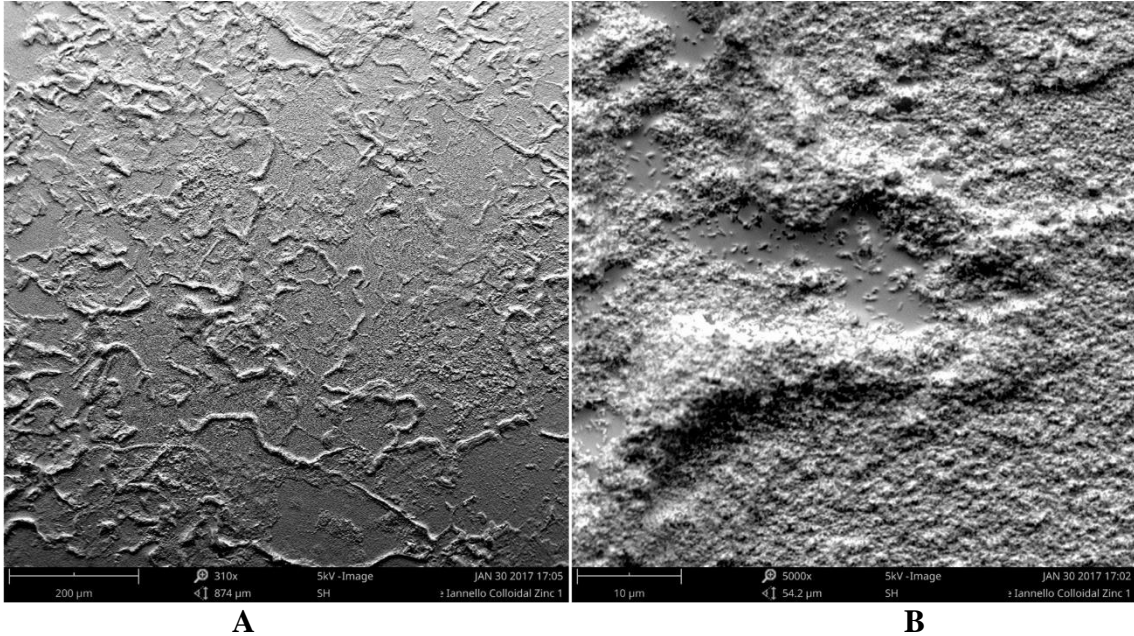
Figure 10. Zinc oxide nano-rods on a glass substrate. Individual rods can be seen from top-down, though the film lacks uniformity.

2.2 Sol-Gel Method

Investigation of the zinc oxide nano-particles revealed several methods of synthesis exist, many of which produce very reliable, uniform films of zinc oxide [33-35]. The most common method involves creation of a sol-gel using a precursor of either zinc nitrate or zinc chloride. A substrate is then momentarily placed into the gel and quickly removed, then the substrate is dried at a temperature, usually around 100 °C, and annealed at a much higher temperature, usually around 400 °C. By investigating structural and optical properties of zinc oxide films, a separate synthesis method was proposed which did not involve annealing at a high temperature [33, 36-38]. A sol-gel solution was prepared by the following method.

A 0.1 molar solution of zinc nitrate was prepared by dissolving 3.2695 g of mossy zinc in a minimal amount of nitric acid, and then adding this to 500 mL of deionized water. A 0.1 molar solution of ammonium hydroxide was prepared by adding 8.81 mL of 25% weight ammonium hydroxide to 491.91 mL of deionized water. The 0.1 molar solution of zinc nitrate was then added dropwise at 1 mL per minute to the 0.1 molar ammonium hydroxide solution, over the course of 15 minutes, for a total of 15 mL of the zinc oxide solution added. The solution was then allowed to sit for 10 minutes, as a sol-gel began to form. After 10 minutes, substrates were vertically dipped, and dried horizontally for 10 minutes at 120 °C for 10 minutes after each dip. A total of five dips were performed, and a visible layer was added to the substrate. Figure 11 presents a detailed description of the film, image (a) shows an overall view of the film, while image (b) represents a closer view. Though zinc oxide nano-rods and particles were present,

they lacked overall uniformity. As uniformity is key to perovskite solar cell performance, other methods were investigated.



A **B**
Figure 11. Zinc oxide films on a glass substrate. Image (a) is an overall view while image (b) is a higher magnification.

A second method of zinc oxide synthesis which was investigated involved a similar method as described above, using a method comparable to known synthesis methods[39]. At room temperature, 2 grams of zinc acetate dehydrate was dissolved in 15 mL of DI water, and 8g of sodium hydroxide was dissolved in 10 mL of DI water. The sodium hydroxide solution was then added dropwise to the zinc solution at a rate of 1

mL/min while stirring at 600 rpm. After the time was up, the solution was stirred for an additional five minutes before 100 mL of ethanol was added to the solution. A sol-gel began to form, which was a semi-transparent white color. Separate glass slides were dipped in this solution one time, and four times, and dried at 100 °C for 10 minutes after each dip. Though films were not uniform, of interesting note were the slides dipped four times. Four dips provided the most uniform film, but many different phases of zinc oxide were present. Figure 12 (a) details the overall view of the film after one dip, while (b) details the many different repeating crystals phases present in the film after four dips, at a higher magnification. As this film also lacked uniformity, a more mature method of synthesis and deposition was tested.

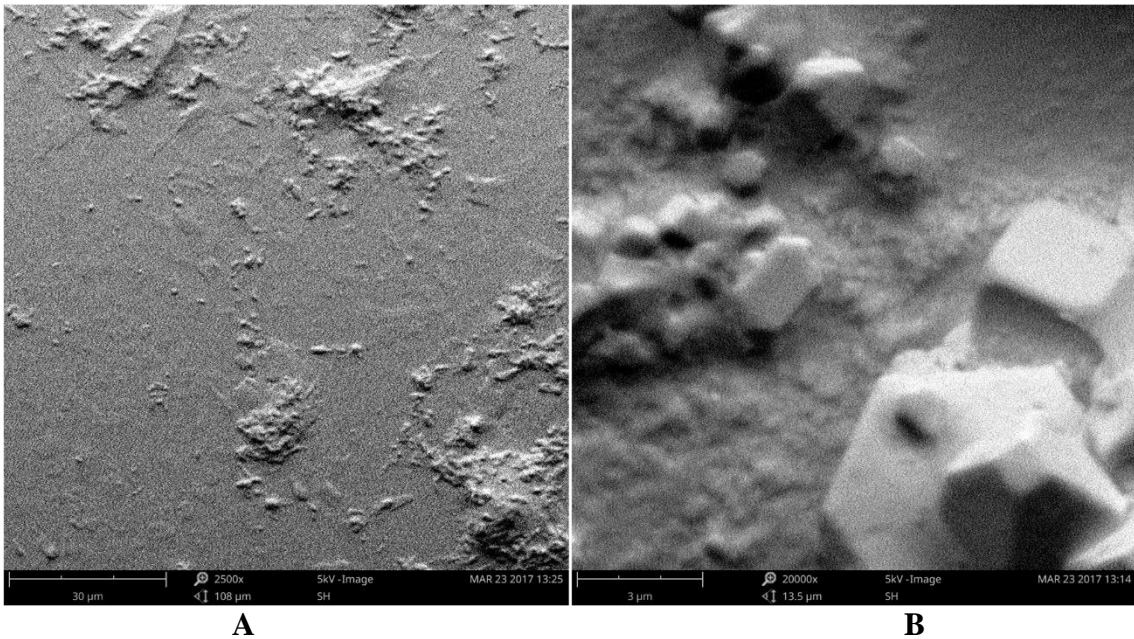


Figure 12. Zinc oxide films. Image (a) is after one dip, image (b) is after four dips.

2.3 Zinc Oxide Nanoparticles

As nanoparticles of zinc oxide can be synthesized with relative ease, a different approach was taken. Stock zinc oxide particles were purchased from Nanoamore, which had an average particle size of 30 nm. As these particles were coated in silicone oil to prevent aggregation, the oil had to be stripped off first. 600 mg of the zinc oxide powder was dispersed in 50 mL of toluene and stirred at 600 rpm for 5 minutes at room temperature. The toluene was decanted off and the zinc oxide was spun in a centrifuge for 5 minutes at 4000 rpm, also at room temperature. The powder was then washed twice with 40 mL of methanol and dried at 80 °C. After this a solution of 65 mL of n-butanol, 5 mL of chloroform, and 5 mL of methanol was mixed, and zinc oxide powder was added to make a solution with a concentration of 6 mg per mL [8]. Figure 13 details the coverage of this film. Even after 5 dips in this solution, there was incredibly poor coverage on all areas of the substrate. As this was very different than previous films, it was decided that synthesized nanoparticles should be used instead of ones purchased from a vendor.

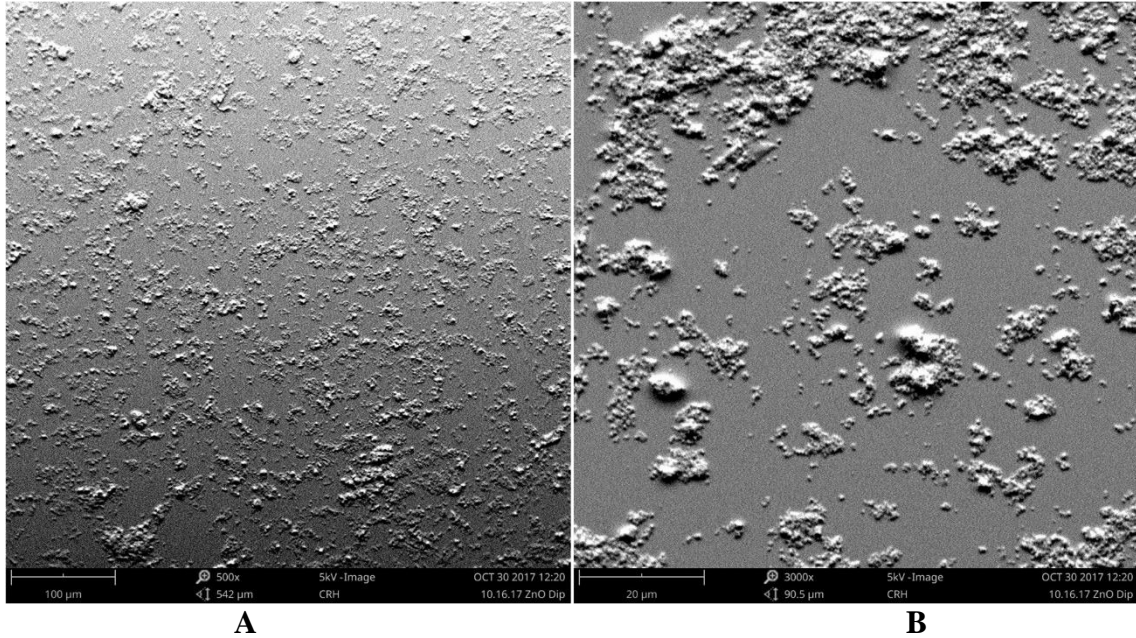


Figure 13. Zinc oxide films from stock nano-particles, (a) presents an overall view while (b) is more magnified.

Nanoparticles were synthesized in the lab according to the literature, and dispersed in the a solution for deposition on a substrate [8]. Glass slides were dipped into the solution between one and five times, with a 3 minute dry at 80 °C between each dip. The films could be visibly seen with the human eye, and were mostly transparent, with coloration towards the edges. The edges of the films were wiped clean while the film was wet during cell fabrication to solve the uniformity issues at the edges. Figure 14 present SEM images of the film after one dip. The film is uniform, with complete coverage of the substrate as seen in image (a). In order to see the film, a scratch was etched into it with tweezers, as seen in image (b) One dip was chosen due to the thickness being closest to the desired value of about 70 nm [8, 40, 41].

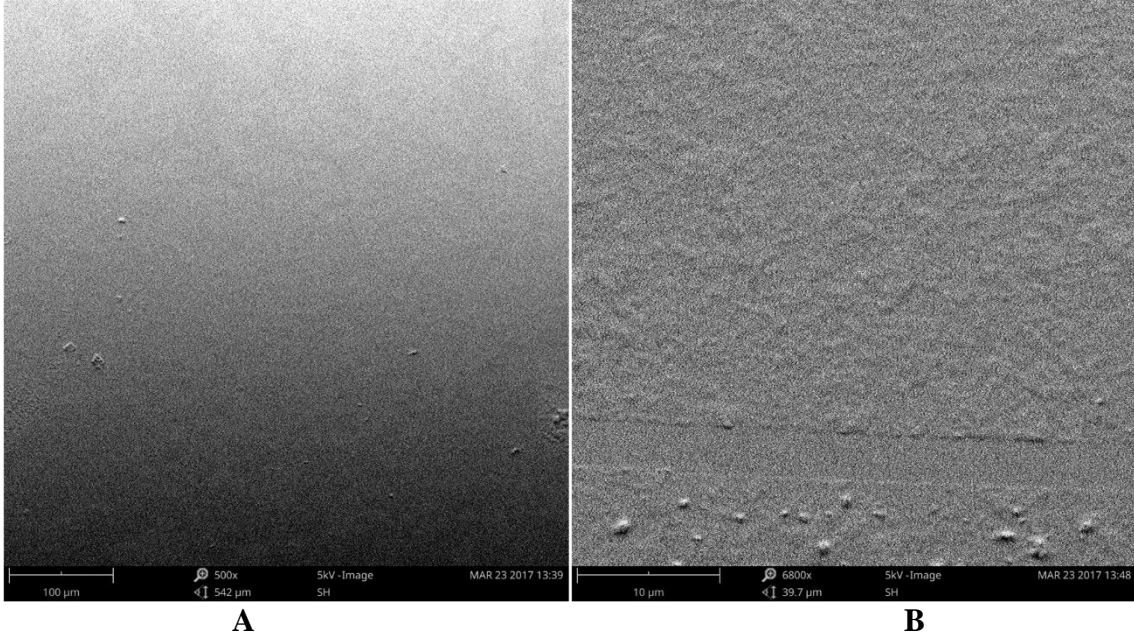


Figure 14. A film fabricated using synthesized zinc oxide nanoparticles. Image (a) presents an overall view, while image (b) shows a closer look.

2.4. Film Thickness and Purity

Using a quartz crystal microbalance (QCM), film thicknesses could be obtained by the following equations.

$$\Delta m = \Delta f / -C_f \quad (2.1)$$

Where Δm is the change in mass per cm^2 , Δf is the change in frequency, and C_f is the sensitivity factor of the crystal at room temperature. Using Δm and dividing by the density of the material allows for the thickness of the film to be calculated. Multiple dips into this solution were performed to see how the effect multiple dips has on film thickness. Figure 15 shows a detailed breakdown of the film thickness relative to dip number. After one dip, the average thickness of a film was about 86 nm, which is close to the normally used thickness of an electron transport layer.

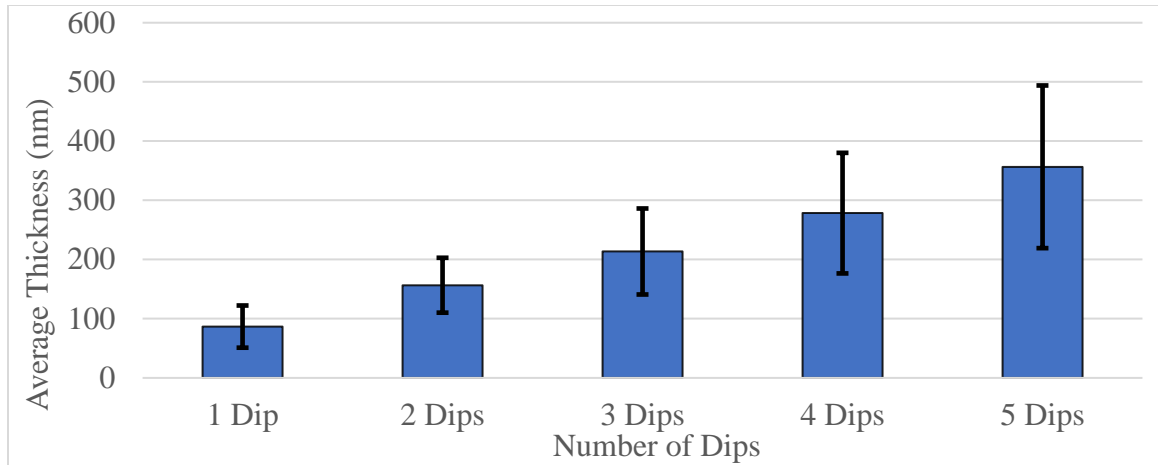


Figure 15. The average thickness of a zinc oxide film after successive dips.

For verification purposes, x-ray diffraction (XRD) was carried out on the film to obtain a diffraction pattern. However, this revealed the film was amorphous, so Fourier-transform infrared spectroscopy (FTIR) was used for verification instead. Figure 16 shows the results obtained by FTIR, and show it is consistent with known values. Of note are the lack of any C-O vibration nodes which would appear around 1500, and C-H stretching nodes, which would appear around 750. This indicates a lack of zinc hydroxide, the most common impurity in synthesis of zinc oxide [42]. As a reliable way of producing the desired ETL was fabricated via dip-coating, the next step was to move onto the next layer, which is the perovskite layer itself.

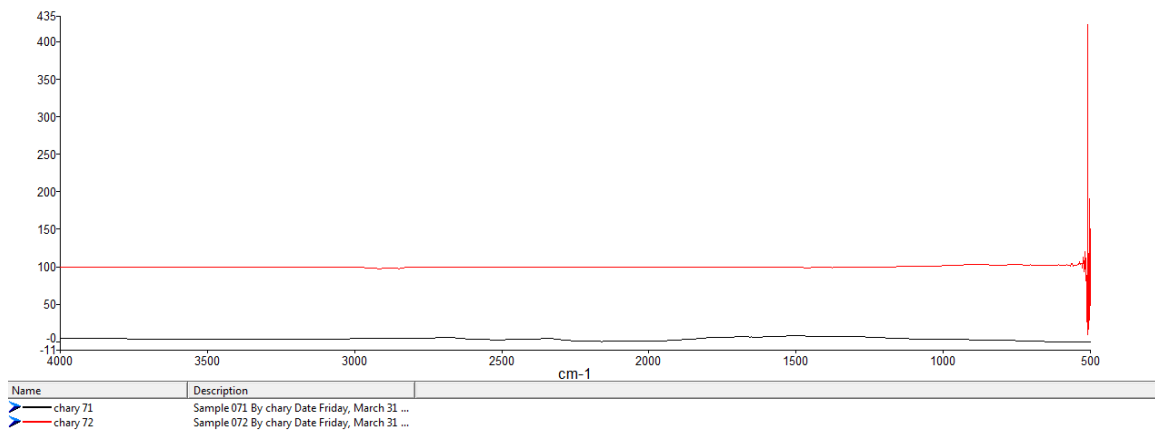


Figure 16. FTIR of the synthesized zinc oxide powder. The lack of any spectra lines at 1500 and 750 indicates a high purity of zinc oxide.

Chapter 3

Lead Iodide and Perovskite

As perovskite thin films are typically fabricated using two-step spin coating, a similar process was developed for spray coating and dip coating. First, in order to minimize costs, films were fabricated without a solvent, using a two-step dip coating method, in order to test viability. As these films were not within the desired thickness range, a decision was then made to use a solvent in order to assist in deposition. Dimethylformamide and dimethyl sulfoxide, a common two common solvents, were used to dissolve lead iodide in order to test spray and dip coating. Films fabricated by spray coating were prone to large structure formation, while films fabricated through dip-coating were much more uniform. Using these lead iodide films as a precursor gave very uniform perovskite films, which were synthesized at a low temperature in ambient air.

3.1 Lead Iodide

Typical MAI perovskite based films are constructed using a two-step method which involves lead iodide as a precursor film [43, 44]. As low-cost solar cells were the main objective, the aim was to use no or minimal solvents during the initial stages of the project. Using this as a starting point, lead iodide films were created using a two-step coating process with the typical reaction of lead nitrate and potassium iodide, according to equation 3.1.



3.2 Fabrication of Lead Iodide Films Without a Solvent

Aqueous lead nitrate was synthesized by dissolving 0.1 moles of lead powder with a minimal amount of nitric acid, and then adding this to one liter of water and

allowing it to dissolve completely. Aqueous potassium iodide was synthesized by dissolving 0.2 moles of potassium iodide into 1 liter of water. About 100 mL of each of these solutions were put into separate beakers, to avoid cross contamination during fabrication. Glass slides were first dipped into the lead nitrate solution, and then immediately dipped into the potassium iodide solution. After the dip into the potassium nitrate solution, a visible lead iodide film could be seen, the slides were immediately withdrawn, and then dried at 120°C. Film coverage was not complete until after the fifth iteration of dips, after which the processes was stopped. Figure 17 present SEM images of this film. As seen in image (a), coverage was complete, however, image (b) shows there were irregularities in the film when looking at uniformity of coverage and particle size distribution. Of note was the large average particle size, with many particles of lead iodide being around 10 microns in diameter. As most perovskite crystals are smaller in size, a different fabrication method was investigated [14, 43].

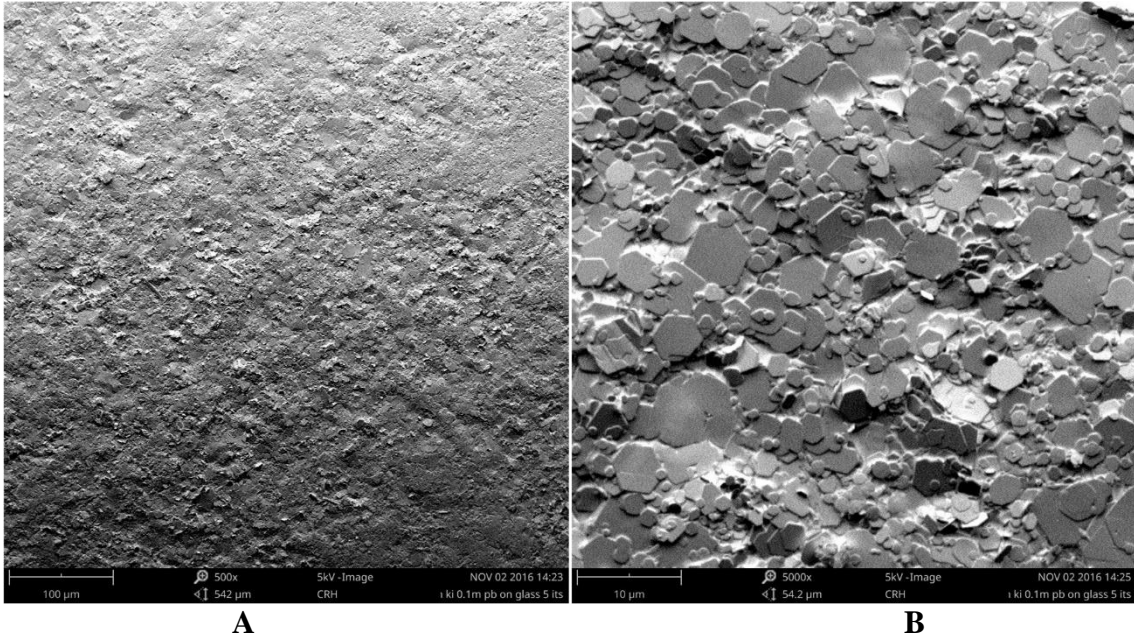


Figure 17. Lead Iodide films fabricated using two step dip coating with no solvent.

Using the previous solutions of 0.1 M lead nitrate and 0.2 M potassium iodide, a colloidal solution of lead iodide could be synthesized. Taking equal parts of the two solutions, combining them, and then removing around 90% of the water, left behind a wet paste which was used for dip coating. For the scale used in the laboratory, usually 50 mL of each solution was used, with 90 mL of water decanted from the final colloidal solution. Glass slides were then dipped at an angle into this solution, and dried horizontally at 100°C. Figure 18 details the film produced using this method. Lead iodide nanoparticles were observed on the substrate, but the film coverage was not uniform, with many holes present through the entire film. With some finesse, a film could be created to cover the substrate uniformly, but it was much too thick. As both methods of lead iodide film synthesis without a solvent did not produce reliable, repeatable results, using a solvent was the next step.

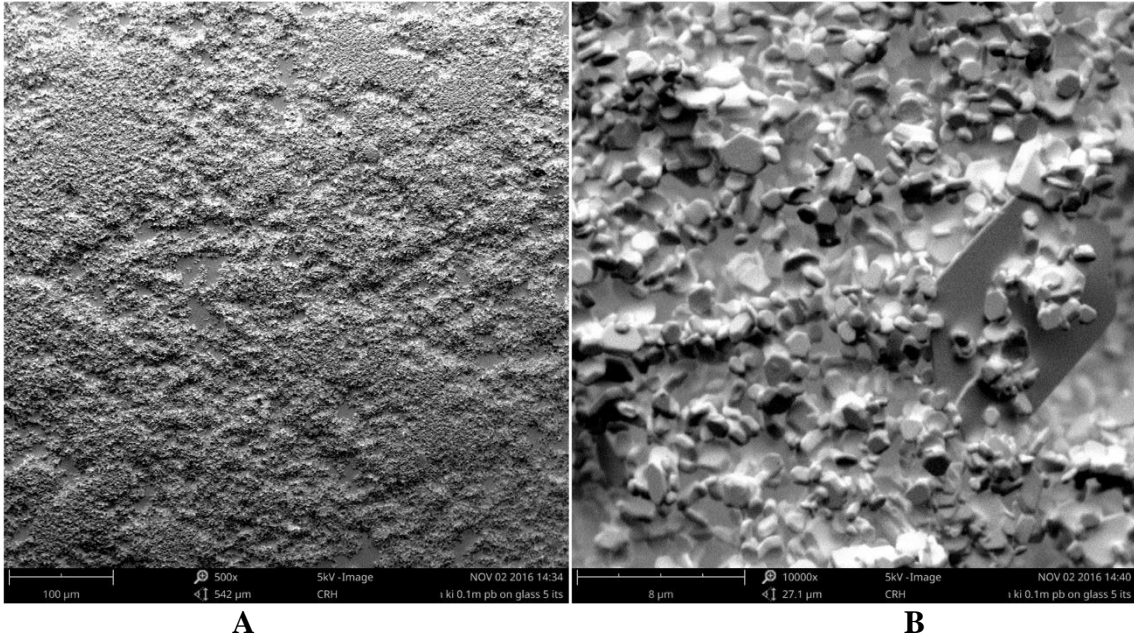


Figure 18. SEM images of colloidal lead iodide films dip coated without a solvent.

3.3 Fabrication of Lead Iodide Films With a Solvent

It has been shown that colloidal particles and spray-coating have a wide variety of applications, not limited to perovskites [45]. As spray-coating perovskite solar cells using lead iodide in a solvent have been constructed in the past, this was used as a starting point [15, 17]. Dimethylformamide (DMF) and dimethyl sulfoxide (DMSO) are the two most commonly used solvents for this purpose, therefore these two solvents were chosen for spray-coating [46, 47]. Films constructed using DMSO are not imaged, as they were visibly non-uniform to the human eye, with lead iodide crystals forming which were multiple millimeters long.

3.3.1. Spray coating. Films were fabricated by using a normal spray bottle and nozzle, which can be found in any laboratory. Firstly, lead iodide was dissolved in DMF

at a concentration of 460 mg ml^{-1} , which is one of the standard concentrations for spin coating lead iodide films for perovskite solar cells [8]. Films were fabricated by spraying on a certain number of sprays, and then drying the substrate at 100°C for about 5 minutes in an oven. Just using one spray covered most of the small substrate, but there were irregularities such as striations and pinholes in the film. As irregularities in perovskite solar cells can drastically hinder performance, more coatings were fabricated to see if these striations could be removed or filled in. Figure 19, image (a) details a film fabricated using three sprays, with a drying in between each spray, which can be compared to image (b) which had a drying step only at the end. When a film is allowed to dry between each spray, the uniformity improves, seen by the lack of pin-holes and striations in the film. However, if too much lead iodide is applied, then micro rods of lead iodide begin to form, which causes non-uniformity in a different way.

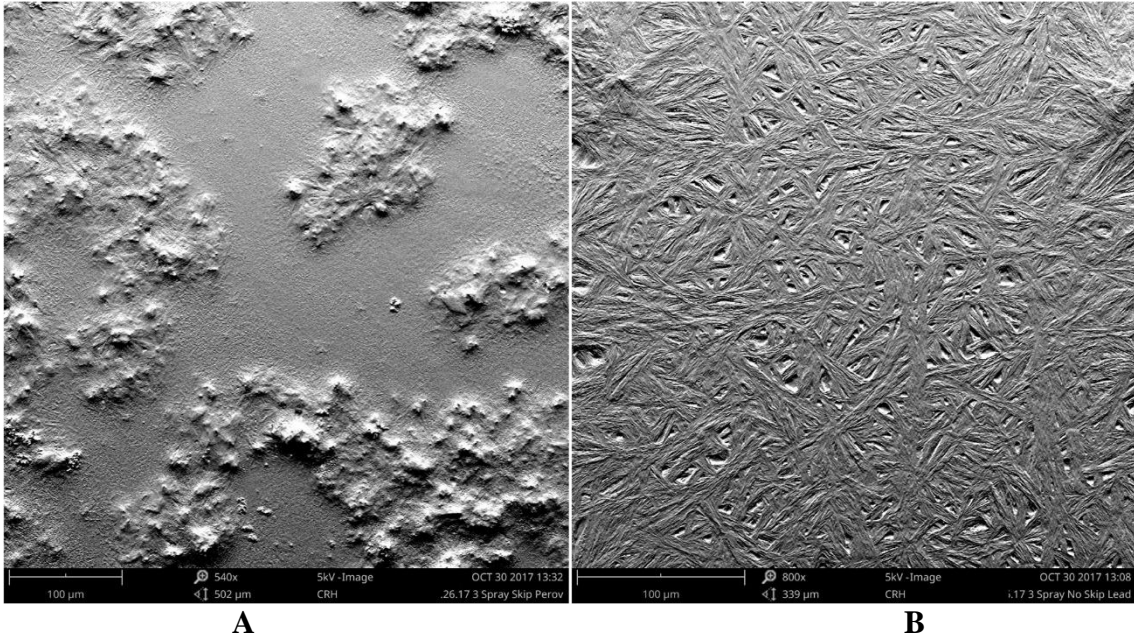


Figure 19. Spray coated lead iodide film fabricated by spraying three times.

Figure 20 shows how this effect can easily be seen, as there are rods of lead iodide measuring well over 100 microns long are present in the films. This figure presents two lead iodide films fabricated using nine sprays. Image (a) had a drying step in between each spray, and image (b) was only dried after all 9 spray were completed. As none of the spray-coating methods showed promising results, a decision was made to see how films fabricated using dip coating with solvents appeared.

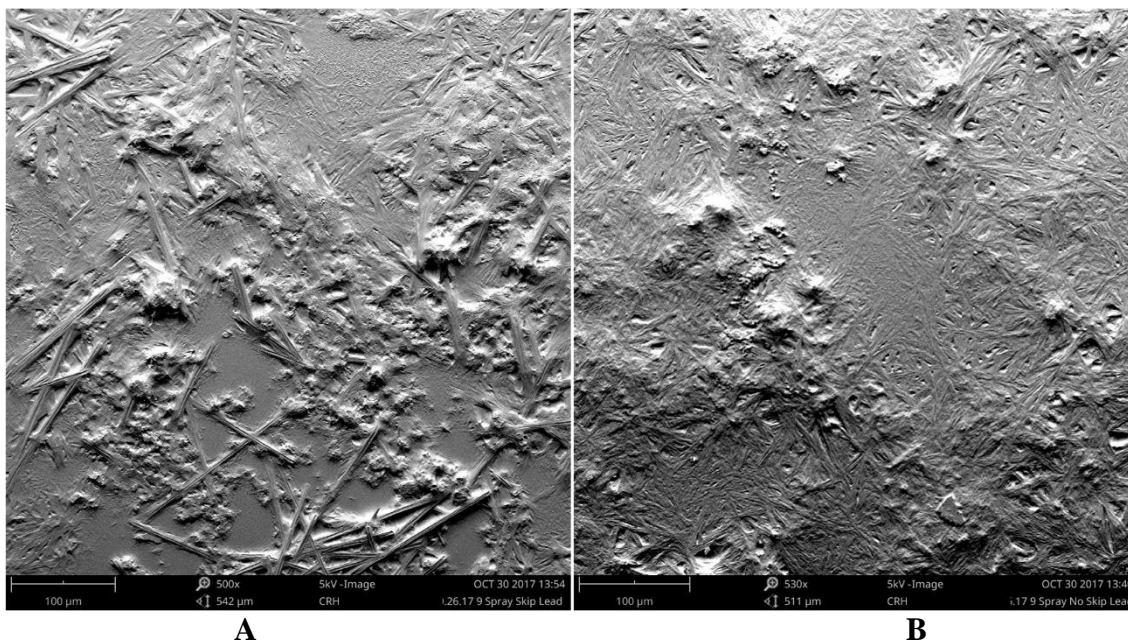
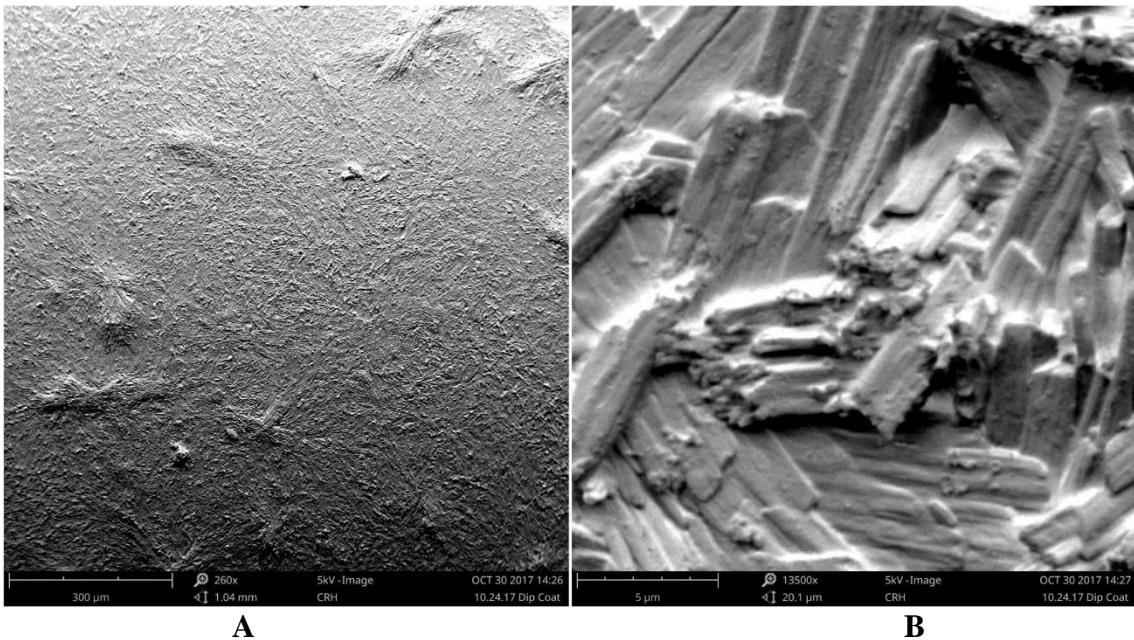


Figure 20. Spray coated lead iodide film fabricated by spraying nine times.

3.3.2. Dip coating. Films fabricated using dip coating showed much more promise than those fabricated with spray-coating. Using the initial concentration of 460 mg ml^{-1} produced relatively uniform films after just one dip at about a 45° angle, and a horizontal dry at anywhere from 80°C to 120°C , with drying time being the only difference with those temperatures. While these films were easily fabricated, there was worry about the thickness of the films, as they seemed visibly thicker than films seen from previous works. Figure 21 shows a film fabricated using this method, and a drying temperature of 120°C for two minutes. While image (a) shows a relatively uniform film, image (b) shows the particles are still quite large. Using a QCM, it was found that films

fabricated in this method has a thickness of about 1 micron, well above the average thickness of 300-700 nm found in most literature [48, 49].



A **B**
Figure 21. Dip Coated lead iodide film using a concentration of 460 mg ml⁻¹ lead iodide in DMF.

While the film was uniform, the thickness was an issue. By halving the concentration of lead iodide, to 230 mg ml⁻¹, it was found that the films were much thinner and more uniform after one drip and drying process. Figure 22 presents the

thickness measurements obtained for a lead iodide film fabricated at this concentration, and dried for two minutes at 120°C. The average thickness after one dip was about 380 nm, which is well within the desired thickness parameters. Figure 23 presents a higher quality SEM image than previously seen. Image (a) shows the overall view of the film, which is more uniform than the higher concentration. Image (b) presents a closer view, shows the larger micro particles are gone, and there are no pinholes. By looking at these images, one can see that the film is not only thinner when the concentration is halved, the film is also more uniform. As a lead iodide film was created which fits the desired parameters, the next step was turning that film into perovskite, according to equation 1.3.

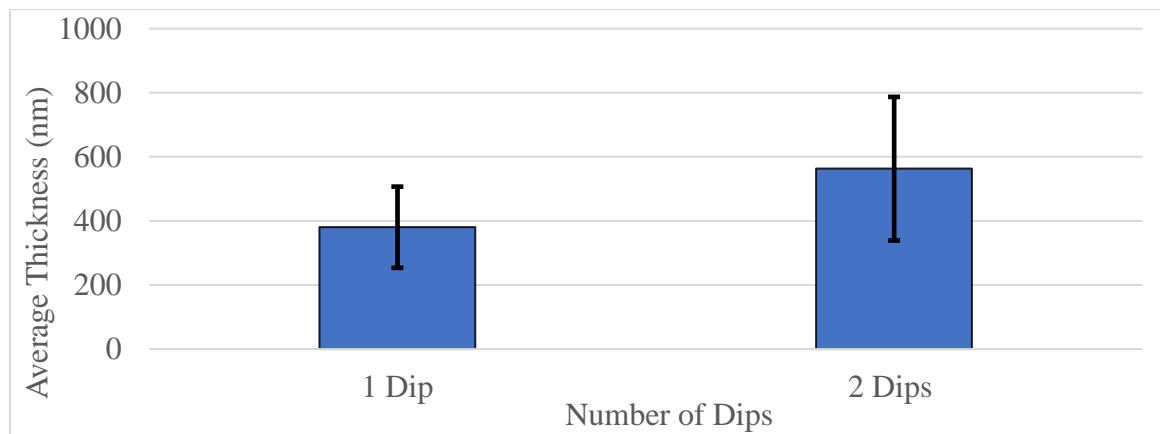


Figure 22. Average thickness of a lead iodide film at 230 mg ml⁻¹ after one and two dips.

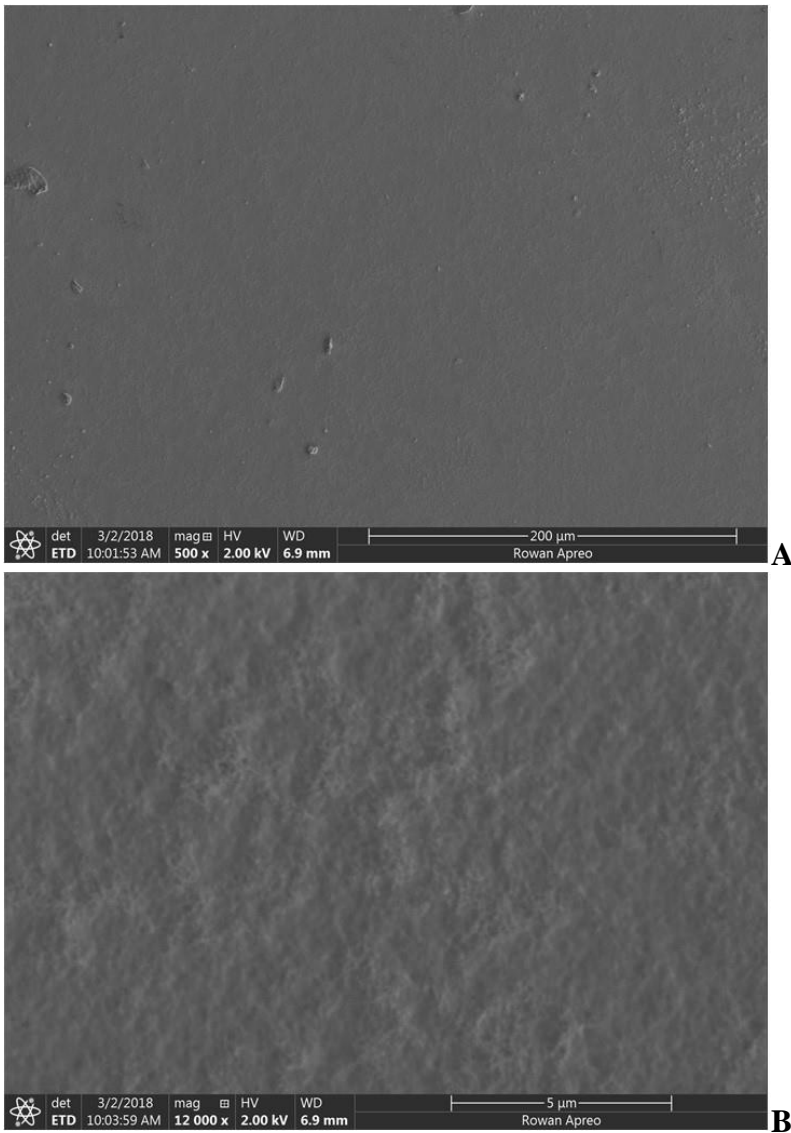


Figure 23. Dip coated lead iodide film fabricated using a concentration of 230 mg ml⁻¹ lead iodide in DMF.

3.4 Perovskite Synthesis

Perovskite films synthesized via a two-step reaction are typically characterized using XRD. A sample was prepared using colloidal lead iodide as seen in figure 18, and reacted by dipping the film in a solution of MAI in 2-propanol at a concentration of 10 mg ml⁻¹ for five minutes, and then drying the film at 80°C for five minutes. The resulting

film was then characterized using XRD, and a diffraction pattern was obtained. As a further verification of the reaction, the film was also analyzed via SEM, and while there were pinholes present, the film was very uniformly cubic. Figure 24 shows a view of this film using an SEM in image (a), along with the diffraction pattern obtained from this film in image (b). The diffraction pattern presented here is consistent with those presented in literature, with the largest peaks seen at 14, 20, and 29, 2θ [11, 50].

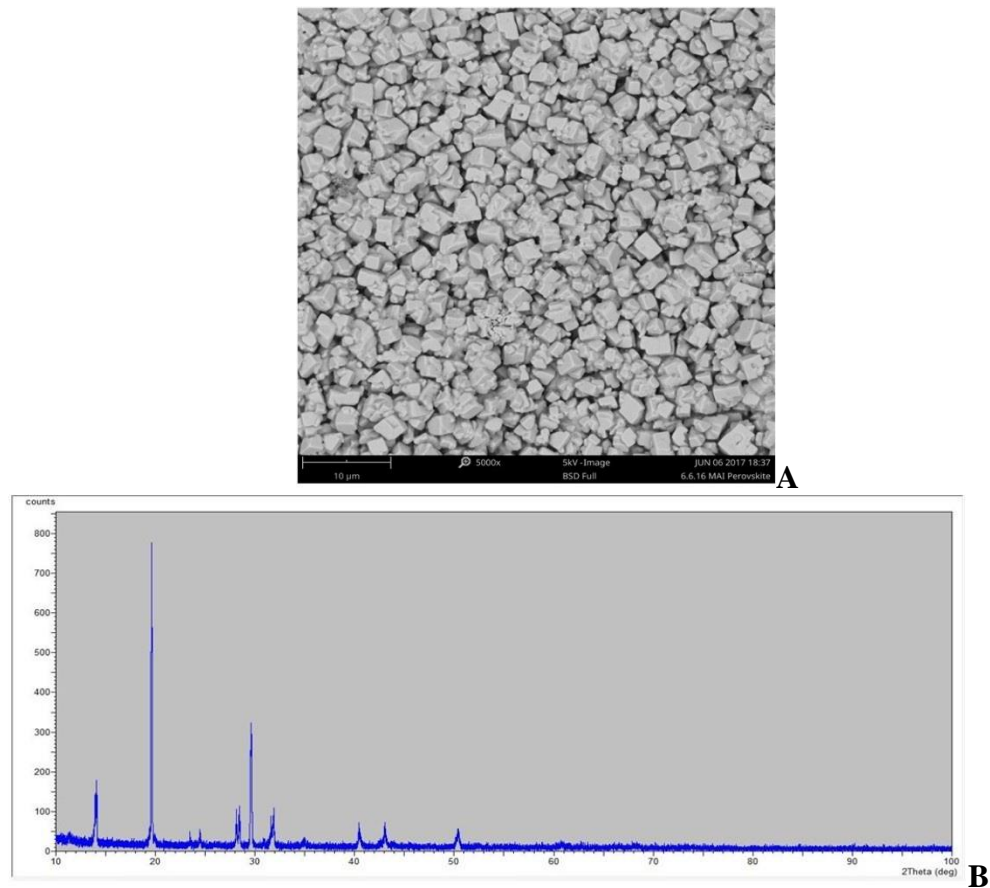


Figure 24. An SEM image and its corresponding X-ray diffraction pattern represented by the two-step dip coated MAI perovskite film.

As pinholes are an inherent problem with recombination between the ETL and HTL, the perovskite films must be annealed to reach their best efficiency [50, 51]. Lead iodide films were prepared by two-step coating using DMF as the solvent. Then, MAI was dripped on to the film, with enough for some excess MAI to be present during drying. Films were then annealed for five minutes, after which more MAI was dripped onto the film. The film was then inserted back into the oven to finish the dry and anneal process. The annealing step was originally at a lower temperature of 90°C, however, this temperature proved to be too low, as even after 45 minutes of annealing at this temperature, pinholes were visible in the film. Uniformity of the lead iodide precursor did have an effect on the uniformity of the perovskite, but it was ultimately the annealing step which could remove imperfections at the nano-scale. By increasing the temperature to 120°C and lowering the time to 5 minutes for the first drip of MAI, and then 2 minutes for the second drip, the pinholes were no longer present. Figure 25 shows a comparison between annealing at 90°C for 45 minutes (image (a)), and annealing at 120°C for 7 minutes (image (b)). The film annealed at a higher temperature was more uniform, and the distinctive cubic crystal perovskite phase expected was still present in the film, which shows the film did not degrade at the higher temperature. Films created using this method did not visibly degrade as long as they were kept at relatively low humidity, below 40%. The fabrication of a perovskite film via which was pin-hole free meant that the final two layers could be constructed on top, first the hole transport layer, followed by the top electrode.

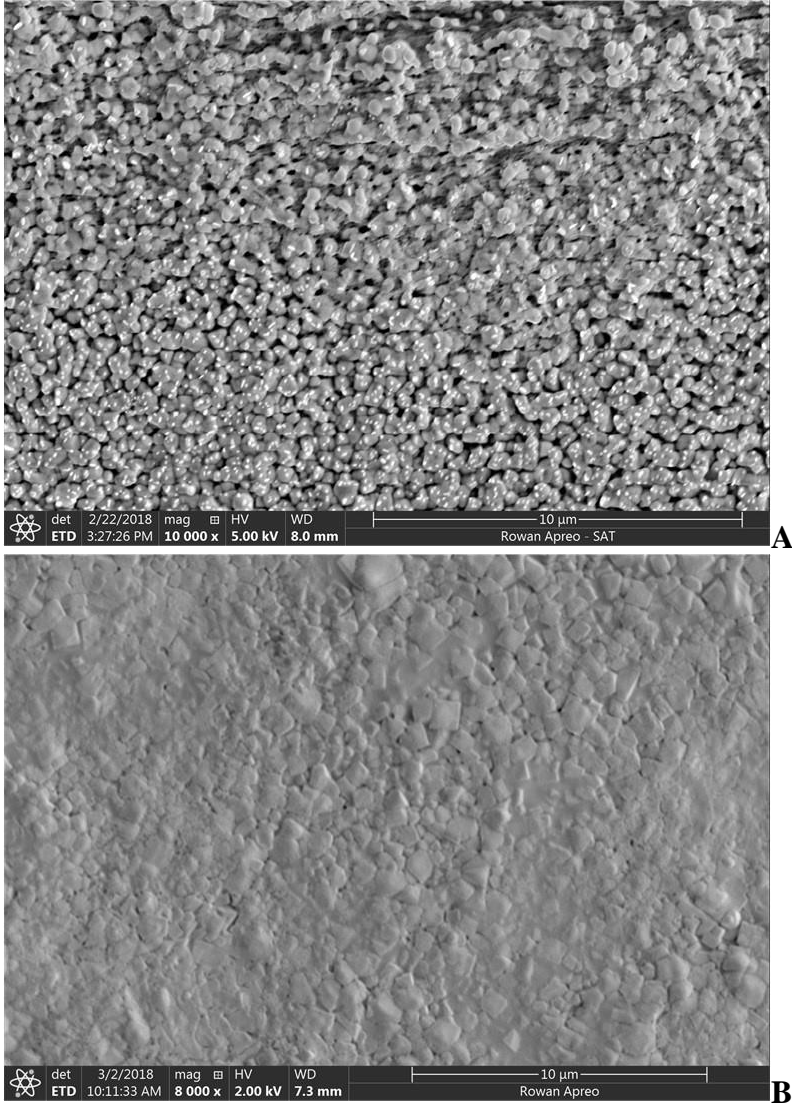


Figure 25. A comparison of perovskite films annealed at two separate temperatures.

Chapter 4

Hole Transport Layer, Top Electrode and Testing

The hole-transport layer is the penultimate layer of the solar cell. The most commonly used material is called Spiro-MeOTAD. Spiro-MeOTAD itself does not allow for the transport of holes, but with the use of p-type dopants, it can. As Spiro-MeOTAD is expensive, an alternative material called copper(I) thiocyanate (CuSCN) was also investigated. The films fabricated using CuSCN were not uniform, and much too thick. As such, even though Spiro-MeOTAD is more expensive, it is the preferred material of choice. The top electrode is usually silver or gold, due to the work function of the metal. Here, silver was used in order to keep costs low. The top electrode is typically deposited using sputtering, but silver paste was also investigated. The best performing cells were ones which had a Spiro-MeOTAD HTL, and a silver electrode deposited through sputtering.

4.1 Spiro-MeOTAD

Referring back to figure 7, following deposition of the perovskite layer, a hole-transport layer must be fabricated on top of it. This layer allows holes to freely pass through it, but does not allow electrons to. Due to this property, there are very few choices of materials, as these are highly specialized. A material called Spiro-MeOTAD ($C_{81}H_{68}N_4O_8$) has been commonly used in perovskite solar cells for years [52, 53]. Spiro-MeOTAD is a highly expensive compound which requires powerful dopants to be used effectively as a hole-transport material, but is unrivaled in its performance [54, 55]. Due to this primary constraint of cost, and the inherent degradation of leftover material, drip coating was investigated for this layer. Literature review conducted about this materials

showed that uniformity is heavily dependent on the previous layer, and slot-die coating had produced uniform films previously [18]. Using this knowledge as a baseline, Spiro-MeOTAD was prepared according to known practices [8]. Spiro-MeOTAD was then dripped onto previously prepared perovskite film 5 microliters at a time, until the whole film was visibly covered. Excess Spiro-MeOTAD was wiped clean, and then the film was placed into an oven at 100°C for two minutes, to allow the film to dry completely. When removed, the film had turned from a dull black, to a shiny black, indicating the Spiro-MeOTAD was present on top of the perovskite. There were no visible ridges present in the film, and figure 26 shows SEM images of this film. Image (a) is an overall view while image (b) is a higher magnification. There are no pinholes present, which shows good uniformity, and recombination is not happening with the ETL through the perovskite.

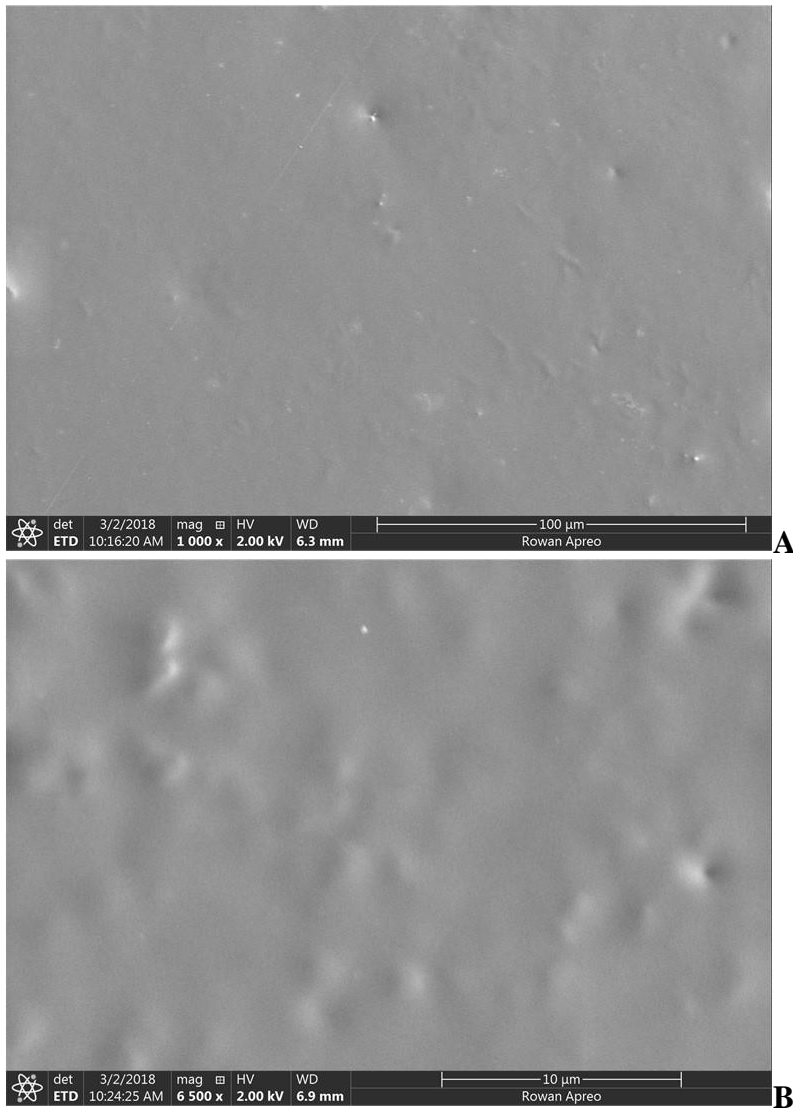


Figure 26. A Spiro-MeOTAD film on top of perovskite.

4.2 Copper(I) Thiocyanate

As lowering costs is one of primary objectives of this research, other hole transport materials were investigated. Of note is one material, copper(I) thiocyanate, or CuSCN. CuSCN is much cheaper than Spiro-MeOTAD, and under some circumstances

may perform better [40]. CuSCN was prepared as in the literature, using ethyl sulfide as a solvent. A reduced graphene oxide (rGO) spacer was also prepared as in the literature, though it took far longer than stated, nearly four days to dissolve rGO in the desired amount of chlorobenzene, instead of a half hour. A CuSCN hole transport layer was deposited by dipping already fabricated perovskite films on substrates into the previously prepared CuSCN solution. The CuSCN did not want to stick to the perovskite after one dip, but after two dips the film was much too thick. Changing the concentration made the film quality worse, with large crystals of CuSCN forming, which degraded the perovskite. Drip coating was also attempted, but the films were much too thick after drying. Figure 27 shows two different types of SEM images of this film. Image (a) shows the many cracks present, while image (b) shows that the cracks do not appear when only looking at a topographical view. These multiple cracks which are present in the CuSCN film could not be fixed with more dips. A decision was made to stick with Spiro-MeOTAD, as this is the standard for hole-transport materials in this field.

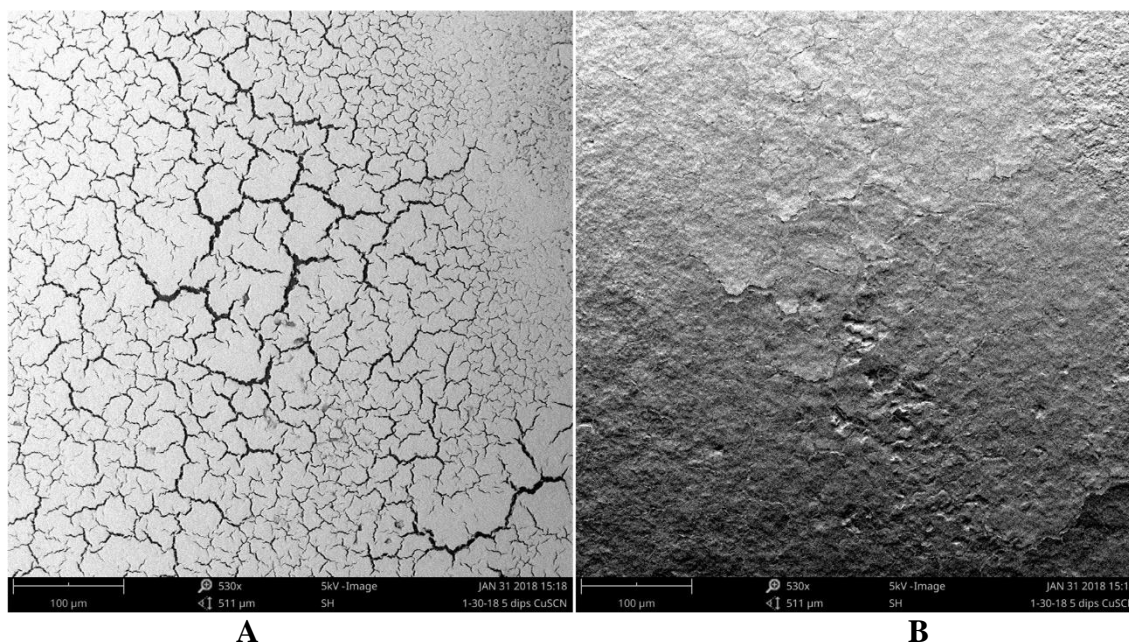


Figure 27. A CuSCN film on top of perovskite

4.3 Top Electrode

Following the HTL is the top electrode, this material is chosen based on the work function of the metal. The work function of a material is defined as the amount of energy needed to move an electron from a point on the surface of a materials, to just above the surface. Referring back to Figure 7, the value of the work function of the top electrode must be around the value of the HTL in order for the perovskite solar cell to function. As such, typical electrodes are made of either gold or silver [56, 57] .The top electrode is typically deposited via sputtering, and is anywhere from 70 -100 nm thick [8, 41]. Sputtering masks were constructed two separate ways, firstly with a 3-d printer, and then with a water jet using thin aluminum sheets. The aluminum masks performed much better, but the process was prone to accidents due to lack of specialized equipment.

First, silver was used as the top electrode, as it is much cheaper than gold. This left the silver prone to oxidizing, which happened multiple times due to things like a broken seal, or the inert argon gas running out. Also, the silver target used was burned through, which showed the biggest flaws in the scalability of sputtering. Due to these inherent problems, an alternative was investigated. Two-part silver epoxy was purchased to connect the top electrode to a wire. The epoxy could not be directly placed onto the cell and cured, as it cuts through the cell to the bottom electrode. A channel was created on a glass slide using clear tape, and the silver epoxy was placed into this channel and then smoothed over with a glass rod. After curing, this created a patch of silver on the glass which was as thick as the channel it was placed in. This could then be placed faced down on top of a fully constructed cell and clamped together. Though results using the paste were not as consistent or efficient as those obtained using sputtering, it is worth investigating in the future in order to lower production costs.

4.4 Testing

Completed cells were tested using a Keithley 2450 sourcemeter, under a Newport solar simulator. The solar simulator was 700 watts per m² on average, but due to variations, the exact measurement was taken each time. As a control, multiple silicon based cells were tested before each perovskite cell, and any offsets obtained were applied to the perovskite. For example, a silicon cell which normally produces 2.5 V and 200 mA under ambient sunlight would only produce 2.3 V and 30 mA under the simulator. The application of this offset was a key component to obtaining accurate results. As of now, only a slight photo response was seen, with a distinct voltage, but lacking current. Future research will attempt to address this problem.

Chapter 5

Conclusions and Future Works

Perovskite solar cells represent a cheaper alternative to silicon based solar cells. Though efficiencies are currently low, there are explainable reasons, which can be fixed. Firstly, zinc oxide as an ETL may work, but it is far outperformed by mesoporous titanium dioxide. Along with this, amorphous zinc oxide does not have a compact layer followed by a mesoporous layer, which can lead to recombination effects. Of note is the fact that zinc oxide has seen less use in the last year where perovskite solar cells are concerned. Even though titanium dioxide requires a higher annealing temperature, and therefore higher cost, it may still be worth it to use over zinc oxide, if the substrate can withstand the high annealing temperatures. More investigations should be conducted on the differences in performance between ZnO and TiO₂, in order to decide which is best.

Perovskite solar cells fabricated via dip coated show promise for the future. Using the methods described previously, a uniform layer of perovskite can be prepared quite easily. Two step dip coating using a solvent is a quick process which is can be easily scaled up to a much larger area. A short annealing step at 120°C allows for full formation of the perovskite to complete, and results in a film which has no holes present. These steps were also completed in ambient air, and cells were stable if sealed using silicone sealant, or kept in a desiccator if unsealed. Thickness appears relatively constant throughout the film, and is dependent on the number of dips, dipping angle, concentration of the solution, and the length of time of each dip. By optimizing these parameters to obtain the best thickness, this process can easily be automated, which can bring production costs to a minimum. Lowering the annealing temperature to be compatible with bendable substrates would also have a huge impact on the feasibility of perovskite

solar cells. This would allow cells to be placed on things such as automobiles and airplanes, as well as uniquely designed buildings which are not compatible with the rigid silicon cells that are currently available. Spray coating, while not viable using the method described here, is another method in which costs may be lowered to a feasible level. By using a finer mist, such as one provided by spray pyrolysis, a more uniform film could be fabricated without micro rods present. It may also be worth it to investigate electrostatic coating of lead iodide, as this is a very mature process already used to create thin films on an industrial scale. Completed films of lead iodide can be bathed in MAI and then allowed to anneal, which is a relatively simple process.

On terms of scalability, the currently used Spiro-MeOTAD as a material for the HTL is the most expensive, and degrades the most rapidly. Methods of recovering unused material should be investigated and optimized before proceeding to large scale fabrication. DMSO and ethanol may provide possible paths to recrystallization and purification of unused Spiro-MeOTAD, which can cut costs drastically. The dopants used with the Spiro-MeOTAD are inexpensive comparatively, but recovery of these materials should also be investigated. Dip coating must also be optimized with this layer, as the methods discussed previously were drip coating based. The use of CuSCN as a material for the HTL did not show promising results. A different solvent for the CuSN other than ethyl sulfide should be investigated, as the CuSCN was prone to crystallization over a large area when used with dip coating. It may be possible that a different method of fabrication would solve this problem, so this should be investigated as well. CuSCN is drastically cheaper than Spiro-MeOTAD, so investigating any possible alternatives are worth it from a development standpoint. Research specific to the materials of the HTL

should be conducted, as this layer and its interactions with the perovskite layer are poorly understood, and insight into the underlying physics of Spiro-MeOTAD would be beneficial.

As currently produced perovskite cells rely on sputtering for the deposition of the top electrode, this is an inherent flaw in their scalability. Regardless of the materials used, sputtering is an expensive process requiring specialized equipment, and typically used to cover relatively small areas. Sputtering over a large area is possible, but not feasible to compete with current silicon solar cell technology. The results discussed here, and in previous works, lend credibility to the use of a separate fabrication process for larger scale. The use of a foil or paste as a top electrode produces comparable results to those obtained from sputtering. Using gold, silver, or aluminum are all viable due to their similar work functions, and creating a performance vs. cost analysis would be useful to decide which material would be best to use. When looking at how perovskite solar cells are tested, results can vary widely based on whether the test was forward or reverse bias, as well as scan speed. Creating a standard way to test perovskite solar cells would be extremely beneficial to the industry. Some cells perform much better if tested under dark conditions first, and then light, or vice-versa. Light soaking and internal capacitance are also factors which can cause measurements to be inaccurate. This has caused many researchers to pick and choose only their best results, and will be a compounding problem if not quickly resolved. An underlying investigation should be conducted on the hysteresis effects of perovskite solar cells, as understanding the mechanisms which cause this could lead to higher efficiencies and more stable cells.

Recombination effects in perovskite solar cells is one of the biggest issues when concerning efficiency. If holes and electrons are allowed to recombine inside the cell, then a potential difference is not created and the cell ceases to function. It is now understood that most recombination happens due to pinholes in the varying layers of the solar cell. If there are pinholes present at any stage, then films may mesh with one another at undesirable locations, which will lead to recombination. If the HTL and ETL are allowed to touch, or somehow bypass one another to touch the opposite electrode, then recombination happens at this junction. Annealing of each layer appears to be a key aspect in preventing pinholes, which was seen most in the perovskite layer itself. An optimization problem can be constructed which is dependent on the length of time and temperature of the annealing step, to determine cost vs. efficiency for this process.

As most current perovskite solar cells are based on MAI and lead, other chemicals should be investigated. This is due to the fact that MAI is synthesized using two chemicals, hydroiodic acid, and methylamine which are on the United States Drug Enforcement Administration list of schedule 1 controlled substances. Because of this, it can be hard to obtain the required chemicals for large scale manufacturing as schedule 1 licenses must be obtained to do so. Along with this, many of the best performing perovskite solar cells contain lead. As such, alternates for this should be investigated using similar elements. By using the Goldschmidt tolerance factor as an initial guide, an optimization problem can be formulated to find out possible combinations of elements which constitute the general ABX_3 form of a perovskite based on their ionic radii. Using the tolerance factor as a guide, A-site modifications can be chosen from there based on their similarity to methylamine. So far, tert-butylamine has been experimentally verified

in also producing a photo response, still using lead as the B site, and iodine as the X site. Other elements similar to lead may be considered for B site modifications, such as tin or bismuth. Along with these, X site modifications can be conducted using other halogens, such as chlorine or bromine. Using these constraints, a list of possible cubic perovskite can be defined, which can then be tests for photo responsiveness. From there, using constraints such as cost and volatility, an optimal perovskite may be defined when looking at cost of fabrication versus efficiency.

References

1. Petroleum, B., *BP Statistical Review of World Energy June 2017*. 2017(66).
2. Administration, E.I., *eia Levelised Cost of Electricity*. 2017.
3. Laboratory, N.R.E., *Best Research-Cell Efficiencies*. 2017.
4. Kojima, A., et al., <*Organometal Halide Perovskites as Visible-Light Sensitizers for Photovoltaic.pdf*>. *J Am Chem Soc*, 2009(131): p. 6050-6051.
5. Johnsson, M. and P. Lemmens, *Perovskites and thin films-crystallography and chemistry*. *J Phys Condens Matter*, 2008. **20**(26): p. 264001.
6. Sato, T., et al., *Extending the applicability of the Goldschmidt tolerance factor to arbitrary ionic compounds*. *Sci Rep*, 2016. **6**: p. 23592.
7. Liu, X., R. Hong, and C. Tian, *Tolerance factor and the stability discussion of ABO₃-type ilmenite*. *Journal of Materials Science: Materials in Electronics*, 2008. **20**(4): p. 323-327.
8. Liu, D. and T.L. Kelly, *Perovskite solar cells with a planar heterojunction structure prepared using room-temperature solution processing techniques*. *Nature Photonics*, 2013. **8**: p. 133.
9. Ye, M., et al., *Recent advances in interfacial engineering of perovskite solar cells*. *Journal of Physics D: Applied Physics*, 2017. **50**(37).
10. Shockley, W. and H.J. Queisser, *Detailed Balance Limit of Efficiency of p-n Junction Solar Cells*. *Journal of Applied Physics*, 1961. **32**(3): p. 510-519.
11. Fu, W., et al., *Controlled crystallization of CH₃NH₃PbI₃ films for perovskite solar cells by various PbI₂(X) complexes*. *Solar Energy Materials and Solar Cells*, 2016. **155**: p. 331-340.

12. Kulkarni, S.A., et al., *Band-gap tuning of lead halide perovskites using a sequential deposition process*. J. Mater. Chem. A, 2014. **2**(24): p. 9221-9225.
13. Hao, F., et al., *Anomalous band gap behavior in mixed Sn and Pb perovskites enables broadening of absorption spectrum in solar cells*. J Am Chem Soc, 2014. **136**(22): p. 8094-9.
14. Liu, J., et al., *High-Quality Mixed-Organic-Cation Perovskites from a Phase-Pure Non-stoichiometric Intermediate (FAI) $_{1-x}$ -PbI $_2$ for Solar Cells*. Adv Mater, 2015. **27**(33): p. 4918-23.
15. Bishop, J.E., et al., *Spray-cast multilayer perovskite solar cells with an active-area of 1.5 cm 2* . Scientific Reports, 2017. **7**(1): p. 7962.
16. Zheng, J., et al., *Spin-coating free fabrication for highly efficient perovskite solar cells*. Solar Energy Materials and Solar Cells, 2017. **168**: p. 165-171.
17. Sandstrom, A., et al., *Spraying light: ambient-air fabrication of large-area emissive devices on complex-shaped surfaces*. Adv Mater, 2014. **26**(29): p. 4975-80.
18. Hwang, K., et al., *Toward Large Scale Roll-to-Roll Production of Fully Printed Perovskite Solar Cells*. Advanced Materials, 2015. **27**(7): p. 1241-1247.
19. Liu, G., et al., *A red anatase TiO $_2$ photocatalyst for solar energy conversion*. Energy & Environmental Science, 2012. **5**(11): p. 9603.
20. Zhao, X., et al., *Aluminum-Doped Zinc Oxide as Highly Stable Electron Collection Layer for Perovskite Solar Cells*. ACS Appl Mater Interfaces, 2016. **8**(12): p. 7826-33.
21. Roiati, V., et al., *Stark effect in perovskite/TiO $_2$ solar cells: evidence of local interfacial order*. Nano Lett, 2014. **14**(4): p. 2168-74.

22. Giordano, F., et al., *Enhanced electronic properties in mesoporous TiO₂ via lithium doping for high-efficiency perovskite solar cells*. Nature Communications, 2016. **7**: p. 10379.
23. Park, H., et al., *Surface modification of TiO₂ photocatalyst for environmental applications*. Journal of Photochemistry and Photobiology C: Photochemistry Reviews, 2013. **15**: p. 1-20.
24. Yang, G., et al., *Preparation of highly visible-light active N-doped TiO₂ photocatalyst*. Journal of Materials Chemistry, 2010. **20**(25): p. 5301.
25. Etgar, L., et al., *Mesoscopic CH₃NH₃PbI₃/TiO₂ heterojunction solar cells*. J Am Chem Soc, 2012. **134**(42): p. 17396-9.
26. Kwon, Y.B., et al., *Formation of ZnO thin films consisting of nano-prisms and nano-rods with a high aspect ratio by a hydrothermal technique at 60 °C*. Current Applied Physics, 2011. **11**(1): p. S197-S201.
27. Gu, Y., et al., *Quantum confinement in ZnO nanorods*. Applied Physics Letters, 2004. **85**(17): p. 3833-3835.
28. Yamabi, S. and H. Imai, *Growth conditions for wurtzite zinc oxide films in aqueous solutions*. Journal of Materials Chemistry, 2002. **12**(12): p. 3773-3778.
29. Battisha, I.K., et al., *Semiconductor ZnO Nano-Rods Thin Film Grown on Silver Wire for Hemoglobin Biosensor Fabrication*. New Journal of Glass and Ceramics, 2015. **05**(02): p. 9-15.
30. Su, Y.K., et al., *Ultraviolet ZnO nanorod photosensors*. Langmuir, 2010. **26**(1): p. 603-6.
31. Witkowski, B.S., et al., *Ultra-fast growth of the monocrystalline zinc oxide nanorods from the aqueous solution*. International Journal of Nanotechnology, 2014. **11**(9-1011): p. 758-772.

32. Das, R., et al., *Controllable gold nanoparticle deposition on carbon nanotubes and their application in immunosensing*. RSC Advances, 2015. **5**(60): p. 48147-48153.
33. Farley, N.R.S., et al., *Sol-gel formation of ordered nanostructured doped ZnO films*. Journal of Materials Chemistry, 2004. **14**(7): p. 1087.
34. Ong, B.S., et al., *Stable, Solution-Processed, High-Mobility ZnO Thin-Film Transistors*. Journal of the American Chemical Society, 2007. **129**(10): p. 2750-2751.
35. Kar, S. and S. Kundoo, *Synthesis and Characterization of Zinc Oxide Thin Films by Sol-Gel Dip Coating Technique*. 2014.
36. Paul, G.K., et al., *Structural, optical and electrical studies on sol-gel deposited Zn doped ZnO films*. Materials Chemistry and Physics, 2003. **79**(1): p. 71-75.
37. Ivanova, T., et al., *Study of ZnO sol-gel films: Effect of annealing*. Materials Letters, 2010. **64**(10): p. 1147-1149.
38. Hafdallah, A., et al., *In doped ZnO thin films*. Journal of Alloys and Compounds, 2011. **509**(26): p. 7267-7270.
39. O'Brien, P., T. Saeed, and J. Knowles, *Speciation and the nature of ZnO thin films from chemical bath deposition*. Journal of Materials Chemistry, 1996. **6**(7): p. 1135-1139.
40. Arora, N., et al., *Perovskite solar cells with CuSCN hole extraction layers yield stabilized efficiencies greater than 20%*. Science, 2017. **358**(6364): p. 768-771.
41. Chen, H., et al., *Enhanced Performance of Planar Perovskite Solar Cells Using Low-Temperature Solution-Processed Al-Doped SnO₂ as Electron Transport Layers*. Nanoscale Research Letters, 2017. **12**(1): p. 238.

42. Dobrozhan, O., et al., *Substructural investigations, Raman, and FTIR spectroscopies of nanocrystalline ZnO films deposited by pulsed spray pyrolysis*. *physica status solidi (a)*, 2015. **212**(12): p. 2915-2921.
43. Yang, M., et al., *Square-Centimeter Solution-Processed Planar CH₃NH₃PbI₃ Perovskite Solar Cells with Efficiency Exceeding 15%*. *Advanced Materials*, 2015. **27**(41): p. 6363-6370.
44. Fang, R., et al., *The rising star in photovoltaics-perovskite solar cells: The past, present and future*. *Science China Technological Sciences*, 2016. **59**(7): p. 989-1006.
45. Kramer, I.J., et al., *Efficient Spray-Coated Colloidal Quantum Dot Solar Cells*. *Advanced Materials*, 2015. **27**(1): p. 116-121.
46. Wu, Y., et al., *Retarding the crystallization of PbI₂ for highly reproducible planar-structured perovskite solar cells via sequential deposition*. *Energy Environ. Sci.*, 2014. **7**(9): p. 2934-2938.
47. Ying, C., et al., *A two-layer structured PbI₂ thin film for efficient planar perovskite solar cells*. *Nanoscale*, 2015. **7**(28): p. 12092-5.
48. Burschka, J., et al., *Sequential deposition as a route to high-performance perovskite-sensitized solar cells*. *Nature*, 2013. **499**: p. 316.
49. Bi, D., et al., *Efficient luminescent solar cells based on tailored mixed-cation perovskites*. *Science Advances*, 2016. **2**(1).
50. Nenon, D.P., et al., *Structural and chemical evolution of methylammonium lead halide perovskites during thermal processing from solution*. *Energy & Environmental Science*, 2016. **9**(6): p. 2072-2082.
51. Zhang, X., et al., *High-efficiency perovskite solar cells prepared by using a sandwich structure MAI-PbI₂-MAI precursor film*. *Nanoscale*, 2017. **9**(14): p. 4691-4699.

52. Ding, I.K., et al., *Pore-Filling of Spiro-OMeTAD in Solid-State Dye Sensitized Solar Cells: Quantification, Mechanism, and Consequences for Device Performance*. *Advanced Functional Materials*, 2009. **19**(15): p. 2431-2436.
53. Fabregat-Santiago, F., et al., *Electron Transport and Recombination in Solid-State Dye Solar Cell with Spiro-OMeTAD as Hole Conductor*. *Journal of the American Chemical Society*, 2009. **131**(2): p. 558-562.
54. Jeon, N.J., et al., *o-Methoxy substituents in spiro-OMeTAD for efficient inorganic-organic hybrid perovskite solar cells*. *J Am Chem Soc*, 2014. **136**(22): p. 7837-40.
55. Shi, D., et al., *Spiro-OMeTAD single crystals: Remarkably enhanced charge-carrier transport via mesoscale ordering*. *Science Advances*, 2016. **2**(4).
56. Zhang, B., W. Xie, and Y. Xiang, *Development and Prospect of Nanoarchitected Solar Cells*. *International Journal of Photoenergy*, 2015. **2015**: p. 1-11.
57. Noh, J.H., et al., *Nanostructured TiO₂/CH₃NH₃PbI₃ heterojunction solar cells employing spiro-OMeTAD/Co-complex as hole-transporting material*. *Journal of Materials Chemistry A*, 2013. **1**(38): p. 11842.